



Fitzgibbon, T.A., Woodgate, M.A., Jimenez-Garcia, A. and Barakos, G.N. (2019) Validation of the steady state hover formulation for accurate performance predictions. *AIAA Journal*, 57(12), pp. 5293-5308.
(doi:[10.2514/1.J058408](https://doi.org/10.2514/1.J058408))

There may be differences between this version and the published version. You are advised to consult the publisher's version if you wish to cite from it.

<http://eprints.gla.ac.uk/189610/>

Deposited on 04 July 2019

Enlighten – Research publications by members of the University of
Glasgow
<http://eprints.gla.ac.uk>

Validation of the Steady State Hover Formulation for Accurate Performance Predictions

T. A. Fitzgibbon*, M. A. Woodgate[†], A. Jimenez - Garcia[‡], G. N. Barakos[§]
CFD Laboratory, School of Engineering, University of Glasgow, G12 8QQ Glasgow, UK

This paper shows accurate predictions for hover performance regardless of planform geometry, blade tip Mach number or disk loading. To prove this statement, sensitivity analyses were performed along with performance predictions for four rotor designs. Planform effects were also studied, such as blade anhedral, showing the strong sensitivity of the rotor blade performance due to geometric features. The steady state solution methodology with imposed Froude boundary conditions is shown to give accurate results for relatively coarse grid sizes. This approach leads to reduced computational costs compared to time-dependent simulations. It is also recognised that given the current accuracy of the available experimental data, the use of more advanced CFD methods may not be fully justified. To advance the accuracy of modern CFD methods a more comprehensive experimental dataset is required.

Nomenclature

AR	=	aspect ratio, R/c_{ref}
a	=	speed of sound, m/s
C_p	=	pressure coefficient, $(p - p_\infty)/(1/2\rho(\Omega r/R)^2)$
C_f	=	skin friction coefficient, $\tau_w/(1/2\rho(\Omega r/R)^2)$
C_Q	=	torque coefficient, $Q/(\rho(\Omega R)^2\pi R^3)$
C_T	=	thrust coefficient, $T/(\rho(\Omega R)^2\pi R^2)$
c	=	rotor chord, m
E	=	endurance, s
FoM	=	figure of merit, $C_T^{3/2}/(\sqrt{2}C_Q)$
k	=	turbulent kinetic energy, m^2/s^2
M	=	Mach number, V_∞/a_∞
M_{tip}	=	blade tip Mach number, $\Omega R/a_\infty$

*PhD Student, CFD Laboratory, School of Engineering. Email: t.fitzgibbon.1@research.gla.ac.uk

[†]Research Associate, CFD Laboratory, School of Engineering, Email: mark.woodgate@glasgow.ac.uk

[‡]Graduate PhD Student, Email: a.jimenez-garcia.1@research.gla.ac.uk

[§]Professor, MAIAA, MRaES, CFD Laboratory, School of Engineering. Email: George.Barakos@glasgow.ac.uk, corresponding author

N_{crit}	=	amplification factor
N_b	=	number of blades
p	=	pressure, Pa
Q	=	rotor torque, $N\dot{M}$
R	=	rotor radius, m
\mathbf{R}	=	flow equation residual vector
Re	=	Reynolds number, $V_{tip}c_{ref}/\nu$
r	=	local radial position, m
T	=	rotor thrust, N
V	=	velocity, m/s
\mathbf{V}	=	flow equation cell volume
\mathbf{W}	=	flow equation solution vector
y	=	chordwise location or dimensional wall distance, m
y^+	=	dimensionless wall distance, $y\sqrt{\tau_w/\rho/\nu}$
β	=	coning angle, deg
γ	=	turbulent intermittency factor
θ_{75}	=	blade pitch angle at $r/R = 0.75$, deg
Θ	=	local blade twist angle, deg
ν	=	kinematic viscosity, m^2/s
ρ	=	density, kg/m^3
σ	=	rotor solidity (geometric), $\sigma = \int_0^1 \sigma(r) dr$
τ_w	=	wall shear stress, Pa
Ω	=	rotor rotational speed, rad/s
ω	=	k-specific turbulent dissipation rate, m^2/s^3
ref	=	reference value
tip	=	blade-tip value
i, j, k	=	cell index
*	=	sonic
∞	=	freestream value

Introduction

The need for accurate hover simulations has become apparent in the rotorcraft community for a number of years. The power required for hover at high thrust is high and close to the operating limit of the aircraft. Hence, a more efficient rotor design will lead to an expansion of the flight envelope in terms of payload and a larger available power margin in cruise. The value of a rotor design in hover is represented by the figure of merit (FoM). Today, design tolerances in industry are nearing 0.5% in FoM, which represents a payload of one passenger [1], and hence such predictions must be obtainable through CFD. In the past, the majority of novel rotor concepts were investigated via wind tunnel and flight tests. With the current progress of CFD and HPC (High Performance Computing), higher performance rotors are likely to come from CFD and optimisation methods. The accuracy of the employed CFD method is a significant factor in the success of an optimisation process. Another important aspect is the need to balance a rotor design between hover and forward flight. This is one of the reasons why so many different rotor designs are seen across the globe, with examples shown in Figure 1 [2]. A BERP (British Experimental Rotor Programme) planform is used nearly solely in the UK, whereas other regions of the world tend to use simpler designs such as a swept/swept-tapered or a parabolic tips as discussed by Brocklehurst and Barakos [3]. The emergence of more radical rotor designs such as the Blue-Edge blade [4] or the new Boeing rotor blade [5] further show that rotor design is still progressing. CFD has become an important tool to further this advancement and its accuracy in predicting hover performance at limited computational costs must be verified which is the main aim of this paper.



Fig. 1 A wide range helicopter rotor blade planforms showing the variety of used designs [2].

Significant efforts have been performed in the rotorcraft community to study the flow field around a rotor in hover and develop the predictive capabilities of numerical codes. Analytical models such as actuator disk theory and blade

element momentum theory were very quickly seen to have a major drawback - a lack of modelling of the blade-vortex interaction and the effect of the rotor wake. This led to the emergence of prescribed wake models [6, 7] based on empirical relationships, and free-wake analysis, which is based on an iterative calculation of the rotor wake. Low fidelity performance codes were developed using these methods to model the rotor wake along with a blade element momentum theory or potential codes, and are still used today for preliminary performance estimates. They do not, however, rigorously account for the effects of tip shape, nonlinear blade twist and flow separation. Modern CFD analyses, based on Euler and Navier-Stokes methods, have the advantage of direct modelling tip vortex formation and roll-up process, as well as wake convection. One of the key issues for these methods is significant numerical diffusion. In the past, such calculations were considered as computationally expensive, and hence were often coupled with external wake models. With significant developments in CFD methods, including numerical algorithms and grid generation, as well as growth in computational power, today, Reynolds-Averaged Navier-Stokes (RANS) calculations are commonly used for simulation of rotors in hover. With the emergence of advanced rotor blade planforms, Navier-Stokes calculations will be crucial in improving current rotor blade designs.

The current state of the art of hovering rotor calculations is represented by the studies within the AIAA Hover Prediction Workshop formed in 2014 [8]. The selected test case was the S-76 rotor which was experimentally tested by Balch [9], and was chosen due to availability of data for different tip shapes - swept-tapered, rectangular and anhedral. Hence, accuracy of the performance predictions could be compared not only for the swept-tapered S-76 rotor but also, based on the changes due to tip geometry, which are more important when considering rotor design. Code comparisons were made using various solvers of different orders of accuracy, meshing techniques and turbulence models. Various levels of hover performance prediction accuracy were obtained with a number of studies nearing performance predictions within one count (0.01) in FoM. However, a wide degree of scatter, was observed in the blade sectional loads, vortex strength and displacements. Only code to code comparisons could be performed, as only experimental integrated loads were reported. Due to lack of experimental data clear conclusions on which methodologies showed most promise could not be made. Full-Navier Stokes simulations, however, generally gave more accurate predictions, in terms of FoM [10], although at much higher computational costs compared to hybrid techniques or comprehensive analyses. This workshop highlighted the need for a more comprehensive experimental dataset in order to perform more in-depth CFD validation. For this reason, future tests are planned for the PSP (Pressure Sensitive Paint) rotor blade in hover at the NASA NFAC wind tunnel facility. One key aspect of hovering rotor simulations was highlighted by Egolf et al. [11], that due to many modelling simplifications (computational method and setup), compensating errors may be introduced into the results, thus giving perception of good agreement with experimental data. For these reasons, it is important to distinguish which elements of the numerical hover simulation, have a large impact on the overall solution. A number of sensitivity studies have been performed for the S-76 rotor and in view of the future PSP rotor tests, including effects of transition [12–15], different turbulence models [14, 16], installation effects including the fuselage, test stand and facility walls [17],[18]

and aeroelastic effects [18, 19]. These investigations showed which modelling aspects are important and which have a negligible effect on the rotor performance. These considerations, however, must take into account computational costs. For example, modelling the facility walls and test stand will lead to a significant increase in the domain size with negligible **impact on the performance predictions**, whereas transitional effects have a higher sensitivity with a much lower computational overhead.

Another important aspect that can have a large impact on the simulation time is the grid size and solution methodology. The use of different solvers was examined for the S-76 rotor by Jain [20] and Abras and Hariharan [21]. While the integrated loads showed a high sensitivity due to grid refinement, the sensitivity due to the solver used was found to be low, although time-dependent simulations were performed for all solvers. The grid size is associated with resolving the key features of the flow field to capture the correct flow physics. Another grid resolution study [22], examined the mesh sensitivity with a strand grid framework. A study by Hollst and Puliam [23] examined the TRAM (Tiltrotor Aeroacoustic Model) rotor in hover using AMR (Adaptive Mesh Refinement), high order schemes and very large grid sizes of up to 448 millions cells. Chaderijan [1] analysed these results and performed further computations for grid sizes varying from 34 million up to 1.2 billion points. The main conclusion from these studies, was that a very fine resolution of the rotor wake has little impact on the predicted rotor performance, whereas using the DES (Detached Eddy Simulation) turbulence model and/or near-body 5th order spatial accuracy led to much larger improvements in the performance predictions. The difference in the coarse and fine grid solutions in this study was only 0.2 counts in **FoM**. Therefore, accurately capturing the tip vortex formation and roll-up process is much more important, than resolving the far-field rotor wake. Other key issues highlighted were, that RANS solutions tend to lead to high levels of turbulent viscosity in the rotor wake, leading to an under prediction of the **FoM**. Here, this was solved by switching off the viscous terms on the background grid or using the DES turbulent model. Such large grid sizes as used in these studies, cannot support industrial rotor design, especially in combination with optimisation methods, and hence further means of improving the solution time must be sought for.

Periodic boundary conditions and simulating the flow field as steady rather than unsteady lead to major computational cost reductions. In fact, this is how most simulations were performed back in the 1990s and early 2000s, when the computational resources available were much lower than today. The steady hover formulation becomes inadequate if large separated flow regions are seen in the domain. Other possible solutions for reducing the computational costs include coupled Free Wake/Navier-Stokes codes as in [24] or [25]. A study by Narducci [26] compared the unsteady and steady hover solutions for the S-76 rotor with different tip shapes. Here, the unsteady cases were simulated by resolving all four blades on a grid with 63.4 million points whereas the steady state simulations used periodic boundary simulations, leading to a grid size of 16.4 million cells (same grid resolution as for unsteady). Typically, the unsteady state simulations took up to 18 revolutions to converge, whereas the steady state simulations achieved convergence after 30,000 iterations. In terms of performance predictions, both methodologies, achieved comparable predictions (within 1

count in FoM) except at high thrust levels, where the steady state method predicted premature stall, not seen in the unsteady computations or experiments. This is the main limitation of the steady formulation. This method, however, was shown to give accurate performance predictions, in attached flow conditions and only needed 3% of the resources required for unsteady simulations.

The steady state hover formulation is a promising compromise between comprehensive rotor codes such as employed in [27], which employ low fidelity methods, and unsteady RANS simulations in both computational costs and solution accuracy. The steady state method uses assumptions such as periodicity that significantly improve the simulation time, but still uses the RANS equations to accurately capture the tip vortex formation and roll-up effects. For this reason, this method has been utilised in many optimisation studies for rotors in hover [28–31]. Another important aspect to highlight is the fact that while CFD methods and more accurate hover performance predictions are obtained, the accuracy of flight test data and wind tunnel data is not sufficient to validate high-fidelity CFD methods. Examples include, the TRAM rotor experiments [32], the UH-60A rotor experiments and flight tests [33], the SA-365N Dauphin flight tests [34], the B0-105 flight tests [35] and the YAH-64 flight tests [36]. The typical scatter for flight test data approaches 5 counts in FoM, whereas wind tunnel test data is generally able to obtain predictions within 2-3 counts. The scatter in wind tunnel test data is also attributed to facility effects and blade scaling effects for model scale rotor tests. CFD predictions are nearing a scatter of within 1-2 counts, even within many sensitivity analyses. Therefore, the CFD method must capture the correct trends due to planform shape, blade loading and blade tip Mach number to be considered for rotor design applications. The absolute performance value is of less importance, however, predictions must still fall within the experimental data scatter.

To validate, the steady state hover formulation, the method must be evaluated for a wide range of test cases, proving its suitability for a variety of geometries and conditions. The available experimental data must be identified, and based on this a number of test cases must be selected. Before the AIAA Hover Predictions Workshop, the majority of CFD studies for rotors in hover used the Caradonna and Tung experiments [37] or the UH-60A rotor experiments of Lorber [38]. This is due to the fact, that both blades were instrumented and in addition to integrated loads, chordwise surface pressure distributions and sectional loads could be compared with experiment. These two experiments have a significant number of CFD validation studies in open literature and thus will not be considered here. The S-76 rotor blade is also not considered due to an existing wide range of studies within the AIAA Hover Prediction Workshop and the similarity in planform to the PSP blade. Validation of the HMB3 solver for these blades can be found in [39], [40], [19].

In this paper, results for four blade designs are presented using the steady state hover formulation. The PSP rotor blade [12, 41, 42] is selected for this analysis due to available surface pressure data, and further testing planned for in the future for this blade. There is little experimental data for advanced planform validation. To our knowledge, the only experimental data set available is the wind tunnel test performed by Yeager et al. [43] for a blade with a paddle-like tip shape along with a standard rectangular blade. This dataset is used within this paper to validate the method for more

advanced blade planforms as well as comparison with a conventional rotor design. Results for the XV-15 rotor blade [44], presented previously by Jimenez and Barakos [45] are also shown here, to prove the applicability of the method at higher disk loading. These designs, cover the requirements needed to validate a CFD method for rotors in hover, as performance prediction sensitivity due to planform, tip shape, tip Mach number, and blade loading can be evaluated.

Based on past literature studies, it can be stated, accurate hover performance predictions are obtainable with modern high-fidelity CFD methods. However, such calculations are usually associated with high computational costs and cannot support current rotor design needs. With the uncertainties from full-scale experimental/flight test performance measurements, it is difficult to assess the accuracy of modern CFD methods. Therefore, the use of higher fidelity turbulence models and/or numerical schemes along with large grid sizes may not be **fully justifiable for validation**. In this work, the steady-state hover performance prediction methodology is validated for a wide range of test cases with the aims of reducing simulation times, and thus making it a viable solution for industrial design and optimisation.

CFD Method

Fully-implicit HMB3 Solver

The Helicopter Multi-Block (HMB3) [39, 46] code of Glasgow University is used within this study. The HMB3 code solves the Unsteady Reynolds Averaged Navier-Stokes (URANS) equations in integral form using the Arbitrary Lagrangian Eulerian (ALE) formulation for time-dependent domains, which may include moving boundaries. The Navier-Stokes equations are discretised using a cell-centred finite volume approach on a multi-block structured grid. The spatial discretisation of these equations leads to a set of ordinary differential equations in time,

$$\frac{d}{dt}(W_{i,j,k} V_{i,j,k}) = -R_{i,j,k}(W) \quad (1)$$

where i, j, k represent the cell index, W and R are the vector of conservative flow variables and flux residual respectively, and $V_{i,j,k}$ is the volume of the cell i, j, k . To evaluate the convective fluxes, the Osher[47] approximate Riemann solver is used, while the viscous terms are discretised using a second order central differencing spatial discretisation. The Monotone Upstream-centred Schemes for Conservation Laws, which is referred to in the literature as the MUSCL approach and developed by **van Leer** [48], is used to provide high-order accuracy in space. The **HMB3** solver uses the alternative form of the Albada limiter [49] activated in regions where a large gradients are encountered mainly due to shock waves, avoiding non-physical spurious oscillations. An implicit dual-time stepping method is employed to perform the temporal integration, where the solution is marching in pseudo-time iterations to achieve fast convergence, which is solved using a first-order backward difference. The linearised system of equations is solved using the Generalised Conjugate Gradient method with a Block Incomplete Lower-Upper (BILU) factorisation as a pre-conditioner [50]. To allow an easy sharing of the **computational** load on parallel computers, multi-block structured meshes are used. The

Overset grid method is used to allow for the relative motion between different mesh components with the implementation within the HMB3 solver described in [51]. Various turbulence models are available in HMB3 solver, including several one-equation, two-equation, three-equation, and four-equation turbulence models. Furthermore, Large-Eddy Simulation (LES), Detached-Eddy Simulation (DES) and Delay-Detached-Eddy Simulation (DDES) are also available. For this study, the fully-turbulent $k-\omega$ SST model from Menter [52] and transitional $k-\omega$ SST- γ [53] turbulence models are employed. The transitional model is calibrated for low-Mach number flows as in [54], however, has proven to give good predictions here. To reduce the computational expense, the steady state hover formulation is used by assuming periodicity of the flow in the azimuthal direction and using a source-sink model to impose boundary conditions at the inflow and outflow. To account for the rotor rotation, a non-inertial reference frame is used with an additional source term in the momentum equations to account for the centripetal and Coriolis accelerations. The rotor can also be trimmed to a given thrust coefficient value using a hover trimming method. The full description of the hover formulation and trimming method are given in [39].

Blade Geometries

The geometric properties of the four rotor blades considered within this paper are described here: the Langley Baseline (LBL) and Langley BERP blades (LBERP) [43], PSP rotor [42], and the XV-15 tiltrotor blade [44].

The PSP rotor has an aspect ratio (R/c) of 12.2 and a nominal twist of -14 degrees. The blade planform was generated using three radial stations. First, the RC(4)-12 aerofoil was used up to 65% R . Then, the RC(4)-10 aerofoil from 70% R to 80% R . Finally, the RC(6)-08 aerofoil was used from 85% R to the tip. The aerodynamic characteristics of these aerofoils can be found in [55, 56]. The planform of the PSP model rotor has a 60% tapered and 30° swept tip.

The three-bladed XV-15 rotor geometry was generated based on the full-scale wind tunnel model tested by Betzina [44]. The rotor blade planform uses five NACA 6-series aerofoil sections as reported in [57]. The XV-15 rotor blade has a high nominal twist of -40.25° degrees and aspect ratio of 10.71 (R/c). The rotor blade chord is held constant, and extends over almost 80% of the rotor blade. The blade root, however, was not modelled due to the lack of information on the cuff geometry.

Finally, the Langley BERP (LBERP) and Langley Baseline (LBL) blades have the same nominal twist (9° linear twist), radius of 1.428 metres (56.225 inches) and aerofoil sections along the span. The two blades only differ in the tip shape and chord which was increased by 9% for the LBL blade to match the rotor thrust-weighted solidity. Based on the discussion by Perry and Amer [58, 59], the matching of thrust weighted solidity may favour the LBL blade, due to higher geometric solidity (0.101 for LBL compared to 0.096 for the LBERP blade). The RC(4)-10 aerofoil is used inboards of the tip section up to 0.84R, whereas a scaled RC(3)-08 section to 7% thickness was used across the blade tip (RC(3)-07), from 0.86R. The aerodynamics of these two aerofoils are described by Noonan [55],[56]. A linear transition was assumed between the two aerofoil sections. For the LBERP tip, the exact geometric shape and thickness

distribution were assumed. The RC(3)-07 aerofoil was used up to $0.945R$ and then the thickness was tapered off linearly to an assumed trailing edge thickness of $0.04\% c$.

The geometric properties for all of the studied rotor blades are shown in Table 1 whereas the rotor blade planforms (scaled to a chord of 1.0), twist distributions and aerofoil shapes at two radial stations (local pitch angle removed) are shown in Figure 2.

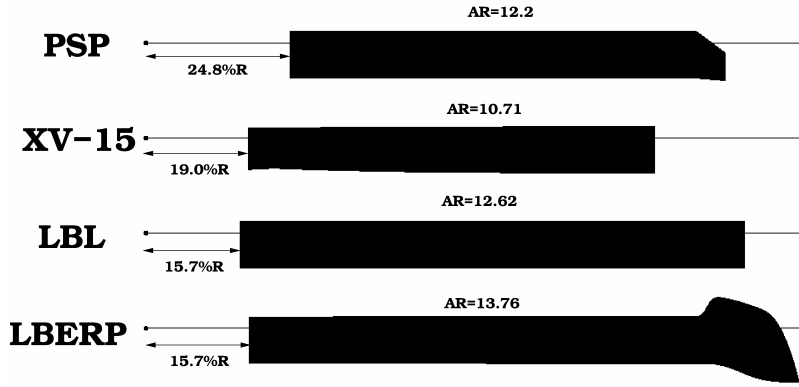
Table 1 Geometric properties for the LBL [43], LBERP [43], PSP [42] and XV-15 [44] rotor blades.

Parameter	LBL	LBERP	PSP	XV-15
Number of blades, N_b	4	4	4	3
Rotor radius, R	1.4281 m (56.224 in.)	1.4281 m (56.224 in.)	1.6891 m (66.50 in.)	3.8100 m (150 in.)
Ref. blade chord, c_{ref}	0.1131 m (4.454 in.)	0.1038 m (4.086 in.)	0.1384 m (5.45 in.)	0.3556 m (14 in.)
Aspect ratio, R/c_{ref}	12.62	13.76	12.2	10.71
Rotor solidity (geometric), σ	0.101	0.096	0.1033	0.089
Linear twist angle, θ	-9°	-9°	-14°	-40.25°

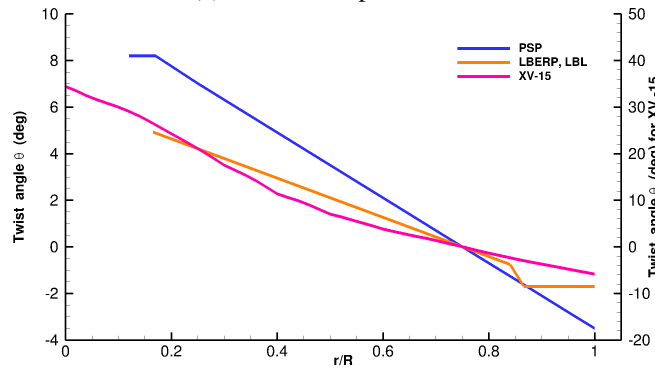
Table 1 shows the rotors under consideration. There are differences in aspect ratio, solidity, linear twist angle and disk loading. Three of the rotors (LBL, LBERP, PSP) are model scale. The LBL and LBERP rotors can be considered as relatively high solidity, low twist rotors. The PSP rotor also has relatively high solidity with a much larger twist. The XV-15 rotor has a much larger linear twist compared to the other blades studied and it also operates at much higher disk loading. Differences can also be seen in the aerofoil sections. Inboard, the PSP and Langley blades used the same section, whereas the XV-15 has a much thicker and cambered section due to operation at much higher loading. The outboard aerofoil section differences are much larger.

Computational setup and Test conditions

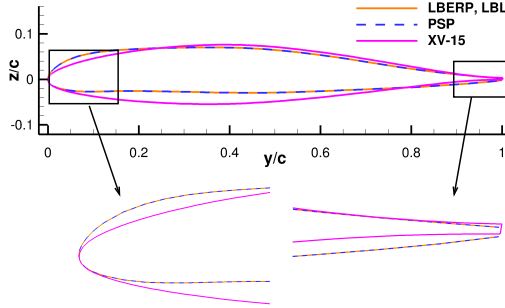
For each of the blades, the chimera technique is used, hence, a foreground grid was generated to resolve the blade geometries, with a background grid to capture the wake. The steady hover formulation is used for the majority of cases within this paper. Hence, only a $1/N_b$ segment is meshed, assuming periodic boundary conditions for the flow field in the azimuthal direction, and the source/sink model is used with Froude boundary conditions imposed at the inflow and outflow. The hub is modelled as a long flat across the entire domain, which is not a realistic representation of the hub. However, as the dynamic pressure in this region is very low, the hub geometry is considered to have a minor impact on the CFD solution. A typical computational domain for these simulations, with the boundary conditions is shown in Figure 3. The typical domain size uses a height of 10-12 rotor radii, and an outflow height as well as radius of 6-8 rotor radii. The domain dimensions come from previous experience using the HMB3 solver [19, 39, 40, 45]. For the blade grids, a C-topology is used around the leading edge of each blade, whereas an H-topology is used at the trailing



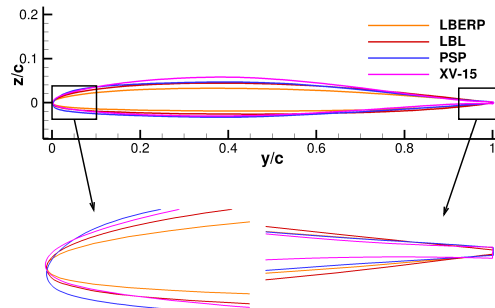
(a) Rotor blade planforms



(b) Twist distributions



(c) Aerofoils at $r/R = 0.75$



(d) Aerofoils at $r/R = 0.95$

Fig. 2 Rotor blade planforms, twist distributions and aerofoil shape comparisons for the PSP, XV-15, LBL (Langley Baseline) and LBERP (Langley BERP) blades used within this study.

edge. The Langley BERP blade has a slightly different topology round the blade tip, as an O-grid was used (compared to an H-grid for the other blades). The employed multi-block mesh topologies for the LBL and LBERP blades are presented in Figure 4, to show the different meshing strategies employed around the tip of the blade. The background grids employ a spacing of up to $12\%c$ near the rotor, with a $6\%c$ spacing to resolve the preceding blade tip vortices. Typically, 160-200 cells are used in the azimuthal direction for the quarter-cylinder domain, leading to a spacing of $8-12\%c$ near the blade tip.

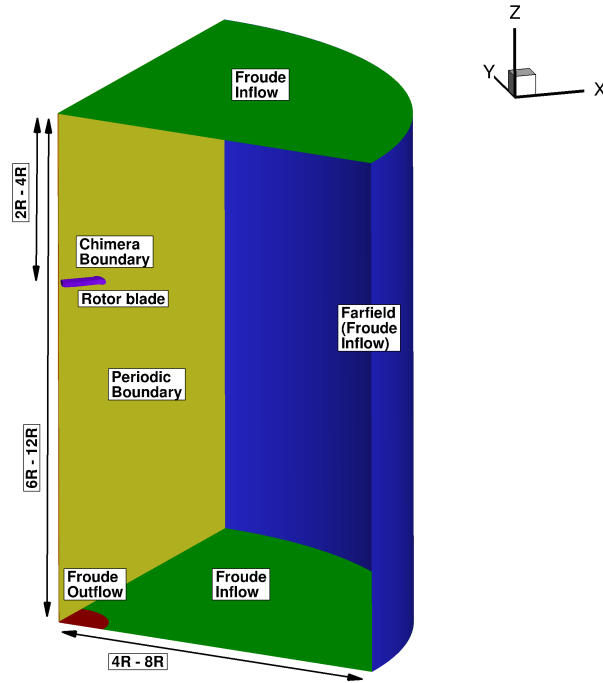


Fig. 3 Typical computational domain for hover simulations using the steady state hover formulation.

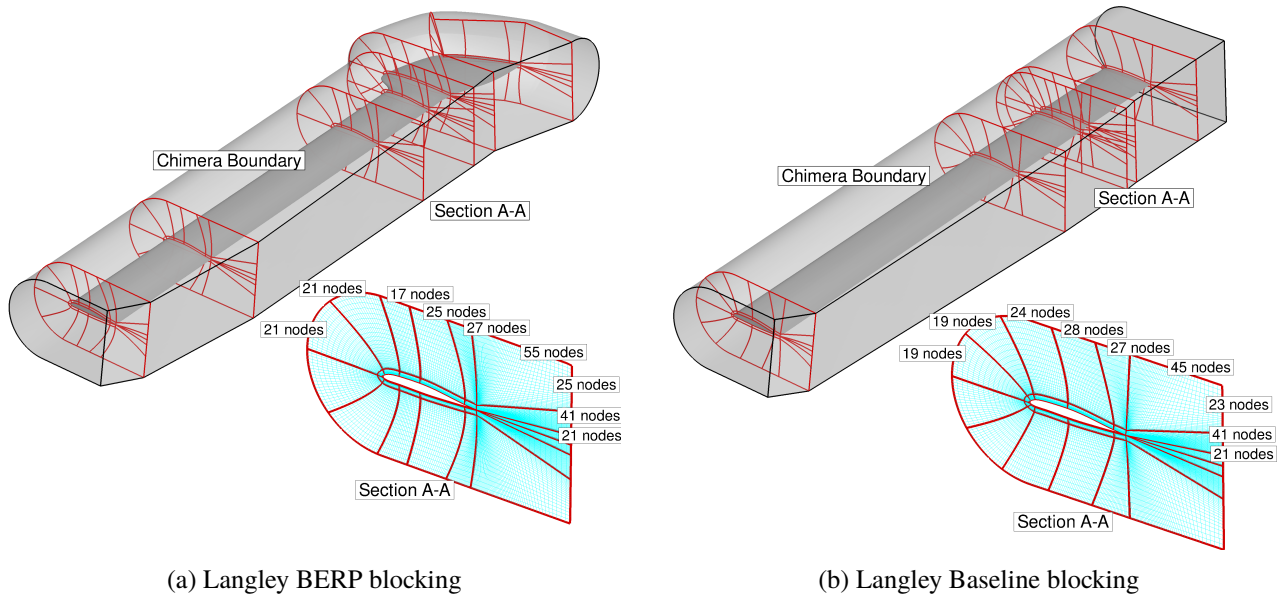


Fig. 4 Multi-block mesh topologies for the LBERP (O-grid round blade tip) and LBL (H-grid round blade tip) rotor blades.

The baseline grid sizes used for each of the blades are shown in Table 2. Additional grids are generated for grid sensitivity study, mainly examining the effect of a finer background grid and are shown in the Table 4. A second mesh was generated for the PSP rotor blade for the transitional model sensitivity studies. The following number of points are

used for grid generation: 220-260 points around the aerofoil (PAERO), 50-65 points normal to the blade (PNORM) and 120-210 points along the span (PSPAN), depending on the geometry complexity. The typical wall distance (WDIST) used is $1.0 \cdot 10^{-5} c_{\text{ref}}$, which ensures a near wall $y^+ \leq 1$. Typically 3.5 to 5 millions points are used for the near-blade grid (FMESH) with 5 to 7 million points used in the background grid (BMESH), giving total mesh sizes (TMESH) of 8.5M to 12 million points.

Table 2 Grid sizes in millions of cells for the simulated rotor blades in hover.

Blade	PAERO	PNORM	PSPAN	WDIST	FMESH	BMESH	TMESH
XV-15	264	48	132	$1.0 \cdot 10^{-5} c_{\text{ref}}$	3.6M	6M	9.6M
PSP (Mesh I)	252	56	215	$1.0 \cdot 10^{-5} c_{\text{ref}}$	5.2M	7.2M	12.4M
PSP (Mesh II)	252	101	215	$1.0 \cdot 10^{-6} c_{\text{ref}}$	8.1M	7.2M	15.3M
LBL	234	64	118	$1.0 \cdot 10^{-5} c_{\text{ref}}$	3.9M	4.9M	8.8M
LBERP	222	66	185	$1.0 \cdot 10^{-5} c_{\text{ref}}$	4.6M	4.9M	9.5M

The simulated cases and test conditions for each of the rotors are summarised in [Table 3](#). The main aim of the selected computations is to cover a variety of collectives, tip Mach numbers and blade geometries. Further information on the exact experimental conditions can be found in the respective references for each rotor blade design: XV-15 [44], PSP [12, 42], Langley Baseline (LBL) and Langley BERP (LBERP) [43].

Table 3 Test cases considered in this paper for the PSP, XV-15, LBL and LBERP blades, Re = Reynolds Number, TM = Turbulence Model.

Blade	M_{tip}	Re	$\theta_{75}(\text{deg})$	$\beta_0(\text{deg})$	TM
XV-15	0.69	$4.95 \cdot 10^6$	3-13	0.0	$k - \omega$ SST
PSP (Mesh I)	0.58	$1.94 \cdot 10^6$	4-12	0.0-3.5	$k - \omega$ SST
PSP (Mesh I)	0.58	$1.94 \cdot 10^6$	6.5-10.2	1.3-3.4	$k - \omega$ SST - γ
PSP (Mesh II)	0.58	$1.94 \cdot 10^6$	6.5-10.2	1.3-3.4	$k - \omega$ SST - γ
PSP (Mesh I)	0.65	$2.16 \cdot 10^6$	9	0.0	$k - \omega$ SST
LBL	0.628	$2.74 \cdot 10^6$	9-13.5	0.0	$k - \omega$ SST
LBL (15 deg anhedral)	0.628	$2.74 \cdot 10^6$	10.5	0.0	$k - \omega$ SST
LBERP	0.628	$2.51 \cdot 10^6$	9-13.5	0.0	$k - \omega$ SST
LBERP (15 deg anhedral)	0.628	$2.51 \cdot 10^6$	10.5	0.0	$k - \omega$ SST

Numerical Results and Discussion

Firstly, sensitivity analyses due to grid size, turbulence models, transition and solution methodology will be presented. Next, the performance predictions for all four blades will be shown in terms of [FoM](#) vs blade loading. Finally, effects of blade planform shape will be analysed.

Sensitivity analyses

Effect of grid size on performance predictions

Two cases were analysed to study the effect of grid size on the **FoM** predictions. The grid sensitivity results for the highly loaded XV-15 rotor were presented previously in [45]. Additionally, a grid sensitivity analysis is performed for the PSP rotor blade. For both blades only the background grid was changed, to examine the effect of rotor wake resolution. The grid sizes for both blades are shown in **Table 4**.

Table 4 Grid sizes in millions of cells for the XV-15 and PSP rotor blades used in the mesh convergence study.

Blade	Foreground Mesh	Background Mesh	Total mesh size
XV-15 (coarse)	3.6M	2.6M	6.2M
XV-15 (baseline)	3.6M	6M	9.6M
PSP (coarse)	5.2M	3.1M	8.3M
PSP (baseline)	5.2M	7.2M	12.4M

Grid convergence for each of the cases is assessed based on **FoM**, thrust coefficient and torque coefficient. The XV-15 blade is analysed at a blade pitch angle of 10° , and the PSP blade is simulated at a higher tip Mach number of 0.65 and three collectives of 6° , 9° and 12° , although no experimental data is available for this tip Mach number. The performance predictions for both rotor blades, at a number of blade loading conditions are shown in **Table 5**.

Table 5 Mesh convergence study results for the XV-15 and PSP rotor blades

Blade	C_T/σ	C_Q/σ	FoM	FoM error
XV-15 (coarse), $\theta_{75} = 10^\circ$	0.1022	0.00890	0.776	1.5 counts
XV-15 (baseline), $\theta_{75} = 10^\circ$	0.1021	0.00897	0.768	0.7 counts
PSP (coarse), $\theta_{75} = 6^\circ$	0.0437	0.00359	0.579	N/A
PSP (baseline), $\theta_{75} = 6^\circ$	0.0444	0.00363	0.585	N/A
PSP (coarse), $\theta_{75} = 9^\circ$	0.0742	0.00652	0.704	N/A
PSP (baseline), $\theta_{75} = 9^\circ$	0.0747	0.00653	0.710	N/A
PSP (coarse), $\theta_{75} = 12^\circ$	0.1060	0.00111	0.702	N/A
PSP (baseline), $\theta_{75} = 12^\circ$	0.1071	0.01121	0.710	N/A

The integrated load results for the XV-15 blade show good mesh convergence, when comparing the resulting **FoM** with experimental data. The **FoM** prediction is within 1 count for the baseline grid. For the PSP blade, experimental data is not available, as these simulations were performed in view of the future tests in the NASA NFAC facility. The differences in the **FoM** predictions with the background grid refinement are lower than 1 count, showing good mesh convergence. **It is expected that, installation and facility effects, as well as the scatter within the experimental test data (wind tunnel or flight tests) will have a stronger effect on the FoM prediction than a finer mesh resolution.** Based

on these observations, it can be claimed that grid sizes of 8-10 million cells are fine enough to obtain good hover performance predictions, within 1 count in **FoM**.

Effect of turbulence model on performance predictions

The effect of different turbulence models is also investigated. For this purpose we use the PSP blade at a blade tip Mach number of 0.585 at 12 degrees collective. The employed turbulence models are the Wilcox $k - \omega$ [60], the Menter Baseline $k - \omega$ [52], and Menter $k - \omega$ SST [52] models. The rotor was not trimmed, however, the thrust coefficient did not change significantly between the three turbulence models. The sensitivity of the rotor performance due to turbulence models was found to be minor, as only a difference of 0.13 counts in Figure of Merit was seen. The integrated loads results are presented in **Table 6**.

Table 6 Integrated loads sensitivity due to employed turbulence models for the PSP rotor at blade tip Mach number of 0.585 and 12 degrees collective.

Turbulence model	C_T/σ	C_Q/σ	FoM
Wilcox $k - \omega$ [60]	0.10285	0.010531	0.7118
Menter Baseline $k - \omega$ [52]	0.10270	0.010497	0.7125
Menter $k - \omega$ SST [52]	0.10259	0.010501	0.7112

Effect of transition on performance predictions

The effect of a transitional turbulence model is examined next. Results for the XV-15 rotor blade were presented in [45] and showed a low sensitivity of the integrated loads due to transition within 1 count of **FoM**. Here, transitional effects are presented for the PSP rotor blade and compared with experimental data of Overmeyer and Martin [12], who measured the integrated loads and transition locations for transition fixed and transition free conditions. For the purposes of examining transition effects on the blade performance, the transitional turbulence model is used, the $k - \omega$ SST- γ model of Menter [53]. The PSP rotor blade was simulated at three thrust coefficients of 0.005, 0.007 and 0.009 using the fully-turbulent and transitional turbulence models. The loads sensitivity due to transition effects is shown in **Table 7**. The results presented, here, used Mesh II with increased wall normal spacing compared to the grid used for the fully-turbulent calculations. The comparison of integrated loads with experimental data and other computational studies is presented later.

Compared to the XV-15 rotor blade, the sensitivity due to transition is much higher for the PSP rotor blade. **This is due to the smaller scale of the PSP rotor blade, and potentially, the milder effect of surface roughness.** The performance improvement due to transitional effects decreases with increasing blade loading. This is due to the fact the transition mainly affects the viscous drag term which is more significant at low loading. The pressure term, however, is of much higher significance especially, at high thrust coefficients. The effect of transition is examined further by comparing the

Table 7 Effect of transition on the predicted **FoM** at three thrust coefficients, $C_T = 0.005, 0.007$ and 0.009 ($C_T/\sigma = 0.0484, 0.0677$ and 0.0871) at $M_{TIP} = 0.585$. FT=Fully-Turbulent; TM=Transitional-Model.

	FoM	Δ FoM
FT, $C_T = 0.00503$	0.608	-
TM, $C_T = 0.00499$	0.681	+7.3 counts
FT, $C_T = 0.00695$	0.678	-
TM, $C_T = 0.00697$	0.742	+6.4 counts
FT, $C_T = 0.00896$	0.710	-
TM, $C_T = 0.00903$	0.768	+5.8 counts

sectional blade loads for the fully-turbulent and transitional cases. The sectional thrust and torque distributions are shown in **Figure 5**. The pressure and viscous contributions to the total torque are also shown. The loads are scaled by blade tip velocity and reference blade chord (equal to the chord of the first aerodynamic section).

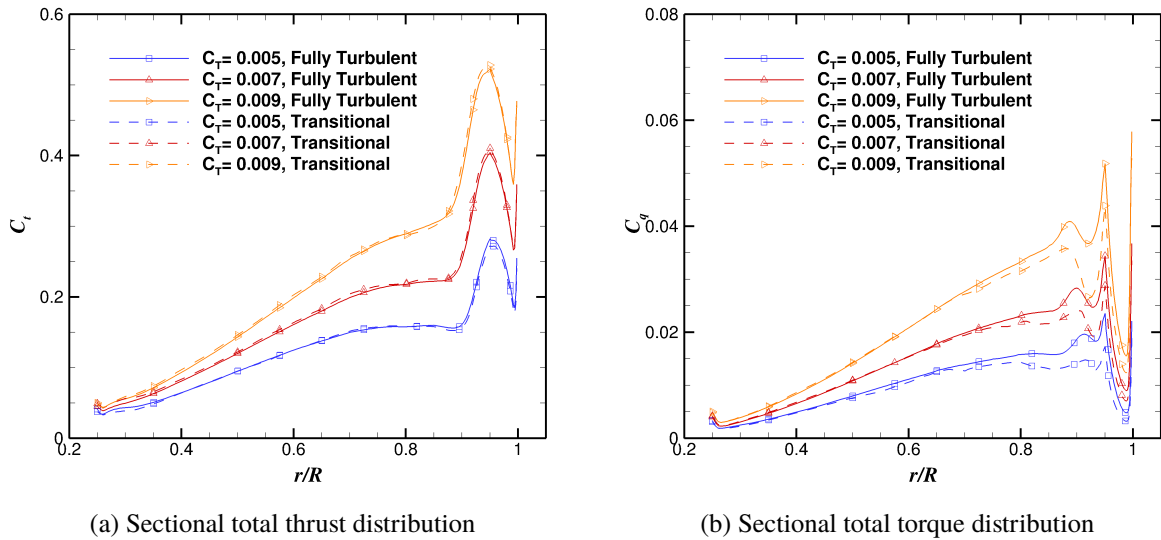


Fig. 5 Effect of transition on the sectional thrust and torque distributions for the PSP rotor blade in hover and three thrust coefficients.

The overall torque is reduced, when accounting for flow transition as expected. This is especially visible in the region where the preceding blade tip vortex interacts with the blade at $r/R = 0.85-0.9$, which is mainly due to the pressure torque term, although the viscous torque contribution is also significantly reduced. The thrust coefficient distributions do not vary as much as the sectional torque. Slight differences can be seen inboards, where slightly higher thrust is seen for the transitional cases. The peak in the thrust also changes with transition, with a minor increase in thrust at higher loading, and reduction at low loading. The effect of transition on the blade loading is examined further by comparing the chordwise pressure distributions at two radial stations of $r/R = 0.75$ and 0.95 , which are presented in **Figure 6**.

The changes in the surface pressure due to transition are subtle. The transition location, can clearly be identified on

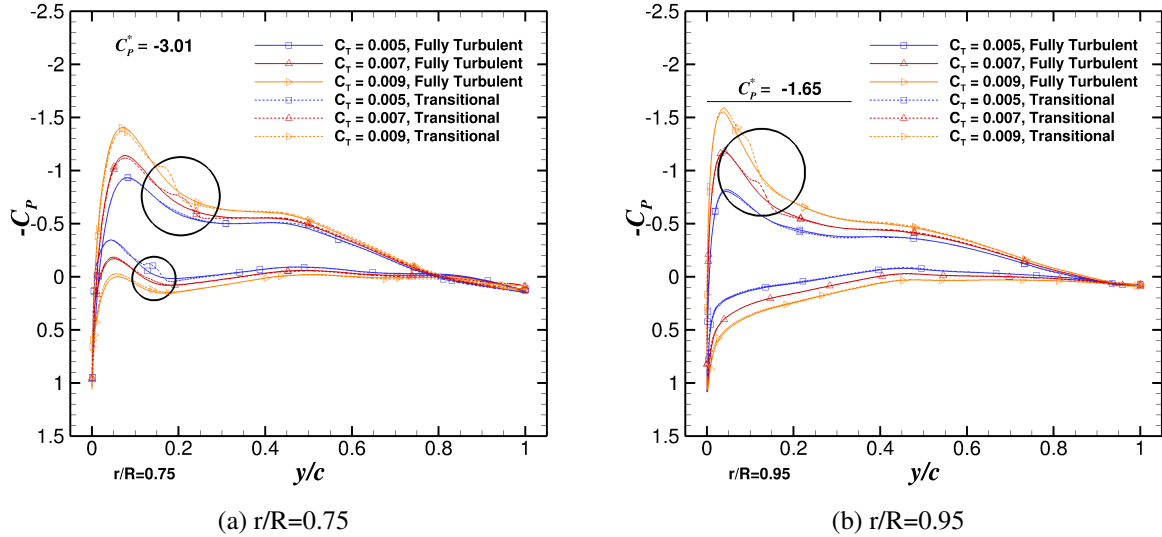


Fig. 6 Effect of transition on the chordwise surface pressure coefficient at two radial stations for three thrust coefficients

the surface pressure graphs, especially on the upper surface at higher loading, where an abrupt change in the adverse pressure gradient is seen. These features are highlighted in Figure 6, by black circles. Changes in the magnitude of the suction peak are mainly noticeable at the highest thrust coefficient, especially in Figure 6 (b). This is in agreement with the sectional loads, where the reduction in suction leads to a reduction in torque due to pressure, at this location. The effect of transition on the surface pressure is not very large, and thus the torque due to pressure does not change as much as the viscous torque term, which approach as much as 40%. This is due to a significantly reduced overall skin friction for the transitional cases. The skin friction contour plots for the upper surface at two thrust coefficients are shown in Figure 7.

Based on these findings, it can be stated that transitional flow effects may be significant for correlation with experimental data at model scale. The importance of including these effects in the CFD simulations, however, varies between each experimental dataset, and depends on the extent of laminar flow encountered on the rotor blade surface. The magnitude of transitional effects will be dependent on factors such as rotor disk loading, rotor geometry, test section turbulence levels and test Reynolds number. Nevertheless, the studies presented here, as well as many CFD predictions in literature obtain good agreement with experimental data using the fully-turbulent boundary layer assumption. For this reason, the information regarding the freestream turbulence conditions and whether the flow was tripped in experimental studies is crucial to obtain good predictions using CFD. In the cases above, a very low turbulent intensity based on a N_{crit} value of 9 and eddy viscosity ratio of 1. Such conditions would not be encountered for full-scale helicopters in flight, due to much higher atmospheric turbulence. Furthermore, vibration, surface roughness and erosion would promote early transition leading to much lower performance improvements as seen for the model scale PSP rotor blade.

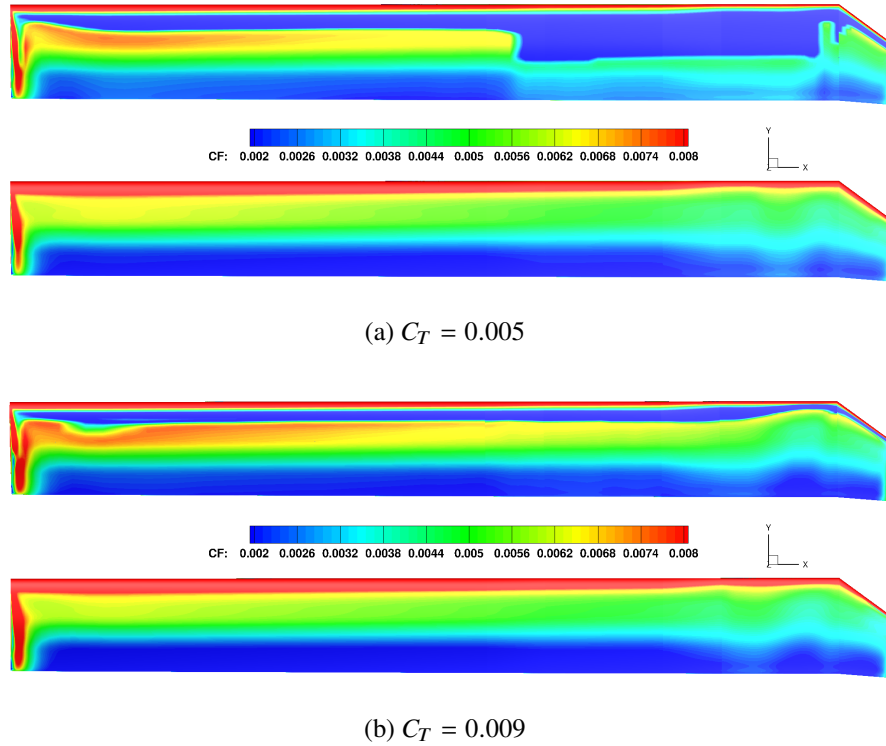


Fig. 7 Effect of transition on the surface skin friction coefficient at low and high thrust, fully-turbulent boundary layer (bottom) and transitional case (top) at each thrust coefficient.

Solution Methodology

Next, the steady and unsteady state formulations are compared. The test case under consideration for this comparison is the PSP rotor blade at 9 degrees collective and blade tip Mach number 0.65. The exact same grid is used, for both simulations of 13.5 million cells. For the unsteady case, the simulation is also run using periodic boundary conditions, so that only one blade is modelled. Farfield conditions are used at the inflow and outflow boundaries. This is the main reason for much higher computational cost of the unsteady simulations, as it takes much longer for the wake to develop. Here, 0.5 degree steps are used in azimuth and the simulation is ran for 30 revolutions. 120 pseudo-time steps are used within each azimuthal time step to achieve good convergence. In comparison, the steady-state simulation is fully converged after 120,000 iterations. The differences in rotor performance are shown in Table 8. The integrated loads for the unsteady simulation are averaged from one revolution.

Table 8 PSP blade hover performance at 9 degrees collective and 0.65 blade tip Mach number.

CFD Method	C_T	C_Q	FoM	% difference
Steady	0.00759	0.000666	0.702	-
Unsteady	0.00760	0.000665	0.704	+0.28%

The performance results for the steady and unsteady formulations are in very good agreement. The difference in FoM is within 1 count. For the unsteady case, a slightly lower torque and higher thrust is predicted. The differences between the two solutions are discussed further analysing the surface pressure distributions and sectional loads. For the unsteady case the data is averaged over one revolution.

The surface pressure coefficient is extracted at two radial stations ($r/R=0.75$ and 0.95) for both solutions and is normalised by the local flow velocity. The comparison for the steady and unsteady cases is shown in Figure 8

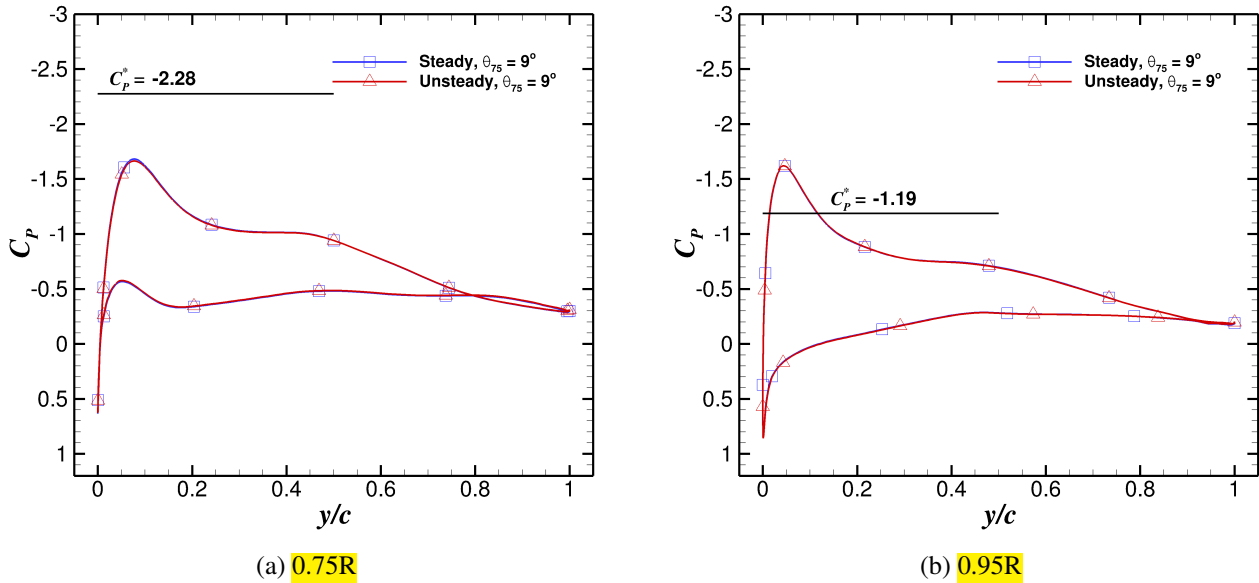


Fig. 8 Comparison of chordwise surface pressure coefficient (normalised by local flow velocity) distributions for PSP blade computed using steady and unsteady CFD formulations.

The surface pressure distributions are in very good agreement. Minor differences can be seen in the magnitude of the suction peaks at the two radial stations, however, these are unlikely to affect the net blade performance to a considerable degree. To analyse the difference in blade loading, the sectional thrust and torque distributions are compared. These are plotted in Figure 9 based on rotor tip velocity.

The sectional loads for the steady and unsteady formulations are in good agreement. Slightly higher thrust can be seen inboards for the steady case. A stronger root vortex is emitted for the unsteady case. Some unsteadiness is also seen in the root region, as the downwash field indicates variation with time. The main cause of this is attributed to the unrealistic representation of the hub geometry, as stated previously, potentially leading to unsteady flow features near the root. Due to the agreement of the sectional torque distributions, the root flow features are not considered to have a significant impact on the net performance of the blade or the flow field in the outboard region. The outboard thrust distribution is also in very good agreement. To highlight the similarity in both solutions, the wake is visualised in Figure 10.

The near-blade wake geometries for both formulations exhibit similar features. A cleaner root vortex can be seen in

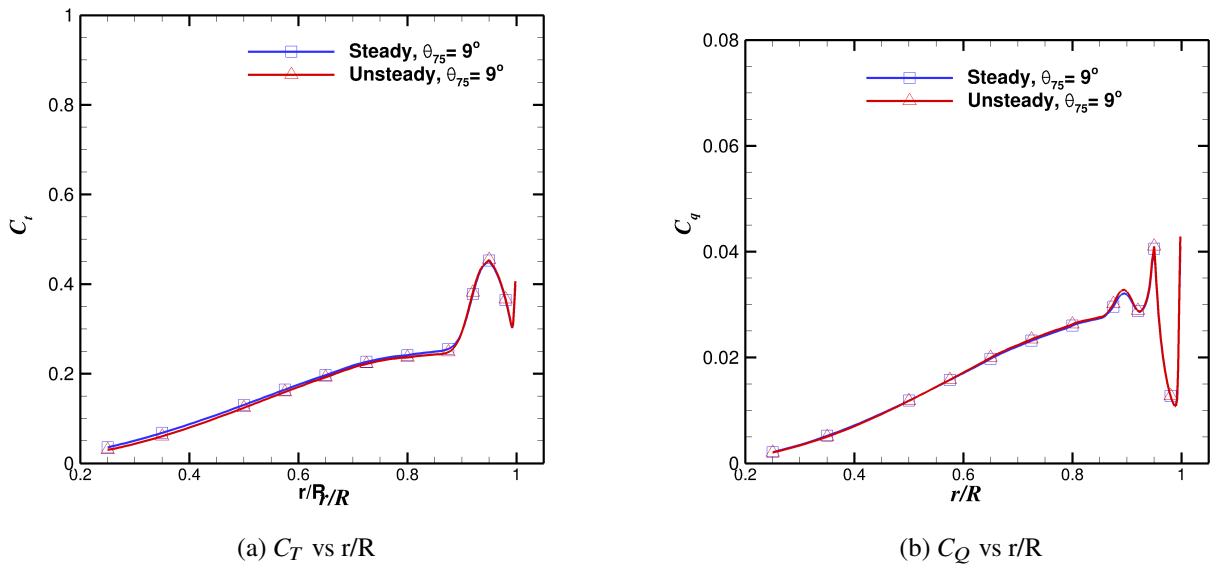


Fig. 9 Comparison of sectional load distributions based on tip velocities for the PSP blade computed using steady and unsteady CFD formulations.

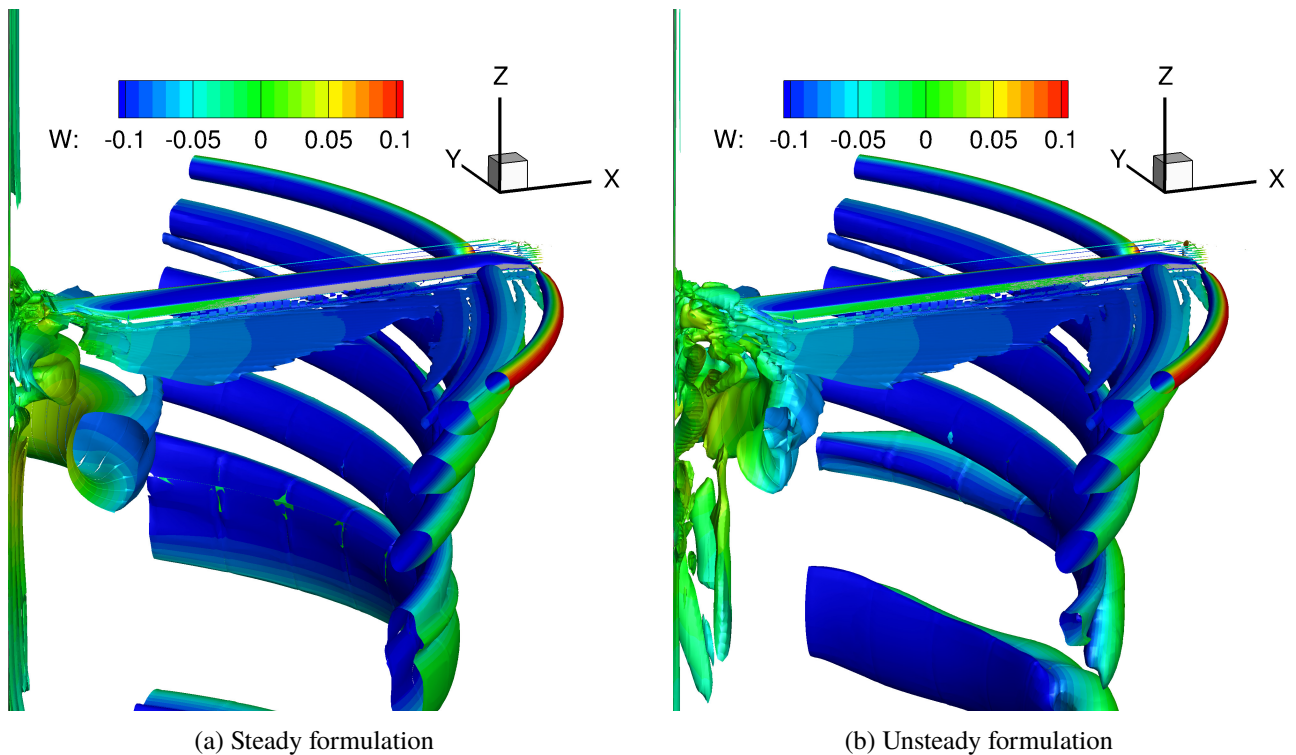


Fig. 10 Comparison of wake geometries visualised using Q-criterion (value of 0.0005) coloured with downwash velocity for the PSP blade in hover computed using steady and unsteady CFD formulations.

the steady case compared to the unsteady case, however, the impact on the predicted performance is not significant as shown earlier. In the unsteady simulation, in the far field, the rotor tip vortices are more distorted compared to the

steady wake geometry. The background **mesh is, however**, coarse in this region, and the rotor tip vortices disappear from the flow field through the action of numerical dissipation. No clear wake breakdown can be seen in either of the cases, a phenomenon that exists in many simulations in literature [11]. Due to the farfield boundary conditions, the wake does not connect to the outflow, and the flow recirculates into the domain which could have a minor impact the blade performance predictions.

The comparison between the steady and unsteady formulations show the validity of the steady state method in accurate hover performance predictions. The steady formulation is able to obtain a similar solution in terms of integrated loads as the unsteady case at significantly lower computational cost.

Performance predictions

Integrated loads predictions

Based on the sensitivity analysis, performance predictions are performed for four blade designs using the $k - \omega$ -SST turbulence model without transitional effects, using grid sizes of 8.5 to 12 million cells and the steady hover formulation. However, comparisons with experimental data are also presented for the PSP blade with free transition. The CFD **FoM** predictions and comparison with experimental data all blades are shown in **Figures** 11-13.

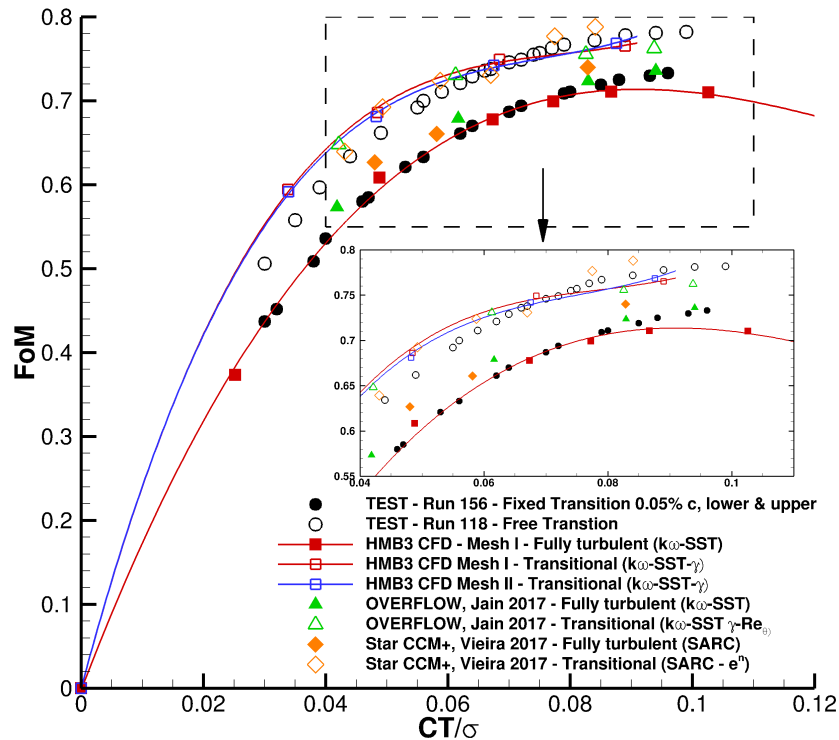


Fig. 11 C_T/σ -FoM for the PSP model rotor at blade-tip Mach number of 0.585 in hover using the fully-turbulent boundary layer and transitional flow assumptions. Comparisons with published CFD data: OVERFLOW [17], Star CCM+ [61] and experimental data [12] are also shown.

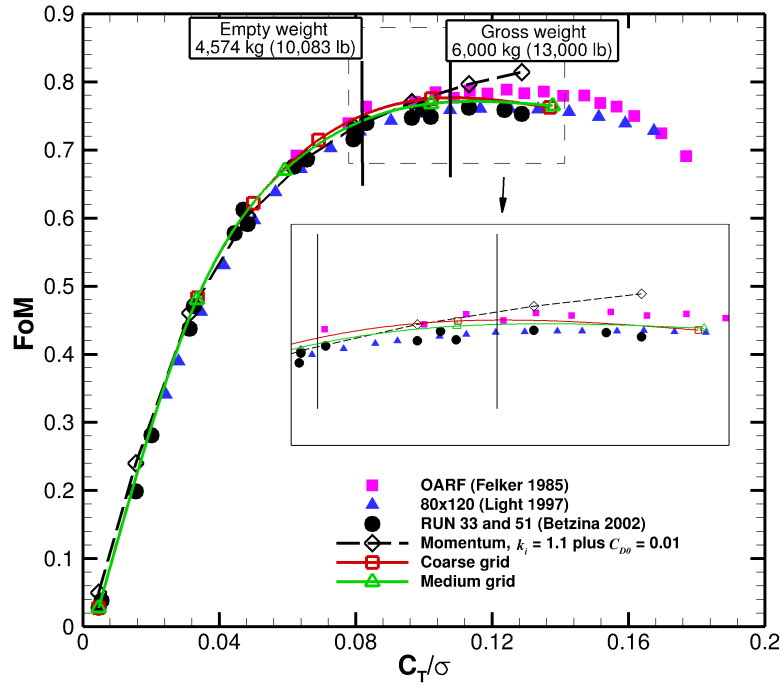


Fig. 12 C_T/σ -FoM for the full-scale XV-15 rotor blade in hover presented in [45] and comparisons with experimental data from Betzina [44], Felker [57] and Light [62].

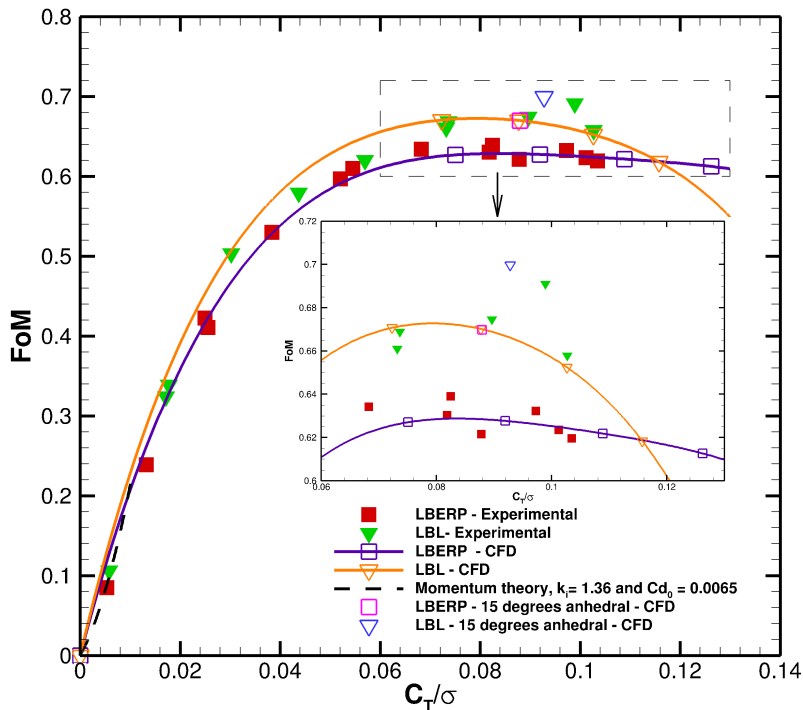


Fig. 13 C_T/σ -FoM for the model scale Langley BERP and Langley Baseline blades in hover and comparisons with experimental data from Yeager et al. [43].

Based on Figures 11-13 it can be stated that the steady state formulation is able to obtain hover performance predictions within experimental data accuracy. Only calibration accuracy was reported (e.g. +/- 0.005-0.01 FoM for the PSP rotor blade), however a larger scatter is seen in the FoM data from experiments. The results for the PSP blade show the importance of transition modelling for model scale blade predictions. Good correlation is also obtained for this blade with other computational studies [17, 61]. At low thrust levels all CFD results show good predictions, however, for the transitional cases, the FoM is slightly overpredicted. In the mid-range thrust levels, excellent predictions are obtained. At high thrust, the scatter between experiment and the three CFD results is larger. The data of Vieira [61] overpredicts the performance, whereas the data of HMB3 leads to an underpredicted FoM. Jain ([17], Figure 10) evaluated the effect of rotor installation on the FoM, and it was found that the installed-rotor FoM presents a higher values (around 1.4 counts of FoM) when compared with the isolated rotor at $C_T/\sigma \approx 0.094$, which perhaps is one of the sources of discrepancy, at high thrust, between HMB3 and experiments. Another potential source of discrepancy could be due to aeroelastic wind up which was not considered here. These differences are still, however, within experimental uncertainty which was reported as between 1 to 2 counts depending on the thrust level. The experimental data scatter is even larger for the highly-loaded XV-15 blade shown in Figure 12, where discrepancies of up to four counts in FoM can be found between the three measured performance results, which can be mainly attributed to different wind tunnel facilities. Felker [57] reported a large recirculation zone during his tests, and perhaps this is the reason for the higher performance in his experimental data set. Once again, excellent agreement is found with the test data of Betzina [44] showing that the CFD method is able to accurately predict the hover performance, at high disk loading and for a highly twisted blade. Finally, the Langley BERP and Baseline predictions also show very good correlation with experimental data. Again, a large degree of scatter is seen in the experimental data points. Performance predictions within 1 count in FoM are unattainable here, due to the much higher experimental uncertainty, which approaches 4 counts for the Langley Baseline blade. Other uncertainties, are present for the advanced Langley BERP planform, in the form of geometric uncertainties. For these reasons, to gain full confidence in CFD validation of hover performance for more advanced planforms, a more accurate experimental dataset is needed and the exact shape needs to be simulated. Here, very good predictions are reported, however, for full validation, other quantities must be compared, such as sectional loads and surface pressure distributions. These results do not exist in open literature for this type of planform. The CFD simulations show the typical behaviour of a blade with this planform shape, as the performance of the Langley BERP blade is able to operate at high loading without significant performance losses. The performance of the Langley Baseline blade rapidly deteriorates at high thrust conditions. However, there is no experimental data to compare with CFD at such a high thrust coefficient. This is in agreement with literature [63],[64] and proves the high angle of attack performance of the BERP blade. The performance of the Langley Baseline and BERP blades with 15 degrees anhedral is further discussed in the section regarding planform effects.

Hover Endurance across blade designs.

To assess the accuracy of the CFD method in more practical terms, the endurance in hover is calculated for each rotor. While the lifting capability of a helicopter may be more important than hover endurance, this performance parameter allows for direct comparison with experimental data across the loading envelope using a single value. For the XV-15 rotor, the representative full-scale aircraft is used for these calculations, whereas for the PSP, Langley Baseline and Langley BERP blades, the tip speed is taken from experiment, whereas the max-take off weight and fuel capacity values are representative of the UH-60A aircraft. The endurance is calculated based on both, CFD predictions and experimental data using equation [65] (based on imperial units).

$$E = \frac{550}{(sfc)(\Omega R)} \int_{C_{T,f}}^{C_{T,i}} \frac{dC_T}{C_Q} \quad (2)$$

where SFC is the specific fuel consumption given in (lb/(rotor hp)/hr), whereas the rotor angular velocity Ω and rotor radius R have unit of rad/s and feet, respectively. The assumed values for each of the rotors are outlined in Table 9. The initial thrust coefficient is based on the max-take off weight of the vehicle, whereas the final thrust coefficient is based on the max take off weight minus the fuel capacity of the helicopter. The endurance values were then calculated based on the CFD predictions and experimental data, and are shown in Table 10. Of course, in reality these values will be slightly different due to performance estimations based on an isolated rotor without accounting for transmission losses, tail rotor or fuselage. Furthermore, the specific fuel consumption data for specific engines is very difficult to obtain. Fuel reserves are also not accounted for.

Table 9 Values used for endurance calculations for each rotor blade design.

Rotor	R	M_{tip}	sfc	Fuel W (lbs)	$C_{T,i}$	$C_{T,f}$
XV-15	12.5ft	0.691	1.0	1436 lbs	0.00953 (13,000 lbs)	0.00850
PSP (UH-60A)	26.83 ft	0.58	1.0	2452 lbs	0.00898 (20,250 lbs)	0.00790
LBL (UH-60A)	26.83 ft	0.628	1.0	2452 lbs	0.00766 (20,250 lbs)	0.00674
LBERP (UH-60A)	26.83 ft	0.628	1.0	2452 lbs	0.00766 (20,250 lbs)	0.00674

Table 10 Comparison of predicted endurance values from CFD and experimental data for each rotor design.

Rotor	E - CFD	E - Experiment	Aircraft
XV-15	57 min	56 min	XV-15
PSP	1h 12 min	1h 11 min	UH-60A
LBL	1h 7 min	1h 6 min	
LBERP	1h 3 min	1h 3 min	

All computed rotors have comparable hover endurance, however the XV-15 aircraft has a much lower aircraft weight, leading to poor hover endurance in its weight class. This is typical for highly loaded tiltrotor aircraft, where hover

endurance is sacrificed for higher forward flight speed. When scaled to the UH-60A aircraft, the PSP blade offers a longer hover duration of 8 and 5 minutes when compared to the Langley Baseline and Langley BERP blades respectively. The comparable hover endurance estimates from CFD and experimental data show that the steady state method is able to accurately predict this performance parameter with limited computational resources.

PSP rotor blade - further validation

The PSP rotor blade was selected for this study due to available surface pressure data and future planned tests in a larger experimental facility. For further validation of the HMB3 code in hover predictions, the surface pressure CFD predictions are compared with experimental data of Wong et al. [41] at two radial stations ($r/R= 0.93$ and 0.99) on the blade upper surface. The C_P is computed based on the local velocity at each radial station:

$$C_P = \frac{p - p_\infty}{1/2\rho_\infty(\Omega r)^2}. \quad (3)$$

Regarding the experiments, two techniques were used to measure C_P distributions, the Kulite pressure transducers (square symbols) and the PSP technique (dashed lines) in [Figure 14](#).

A reasonable agreement is seen by both techniques for both stations at the two thrust coefficients considered here; $C_T= 0.005$ and 0.009 . CFD results are able to predict the overall distribution of C_P at both stations, and the pressure at the trailing edge is also well captured. **However, an overprediction in terms of the C_P magnitude is observed, primarily attributed to missing aeroelastic effects. Aeroelastic blade torsion, for example, could lead to an offloaded blade tip and hence lower C_P in the blade tip region, leading to improved correlation with experimental data.**

Blade planform shape effects

The addition of anhedral showed potential benefits for the S-76 rotor blade [9] as shown within the AIAA Hover Prediction Workshop. Here, we examine the performance improvements for the Langley Baseline and BERP blades with 15 degrees parabolic anhedral at a single collective of 10.5 degrees. The anhedral was initiated at $0.945R$, which is the location where the raked tip begins for the Langley BERP blade. The grids for these blades, were generated from the initial blade grids using a deformation method based on inverse distance weighting. The blade geometry for the Langley BERP blade with anhedral is presented in [Figure 15](#).

The performance results for the Langley Baseline and BERP blades with and without anhedral are presented in [Table 11](#)

The tip anhedral increases the hover performance for both blades. For the Langley Baseline blade, a performance improvement of approximately 3 counts in [FoM](#) is achieved, whereas the Langley BERP blade sees an increase of over 4 counts. Therefore, it can be stated that blade anhedral is more beneficial for the Langley BERP geometry than the Baseline blade. The Langley BERP blade with 15 degrees achieved a similar [FoM](#) as for the standard Langley Baseline

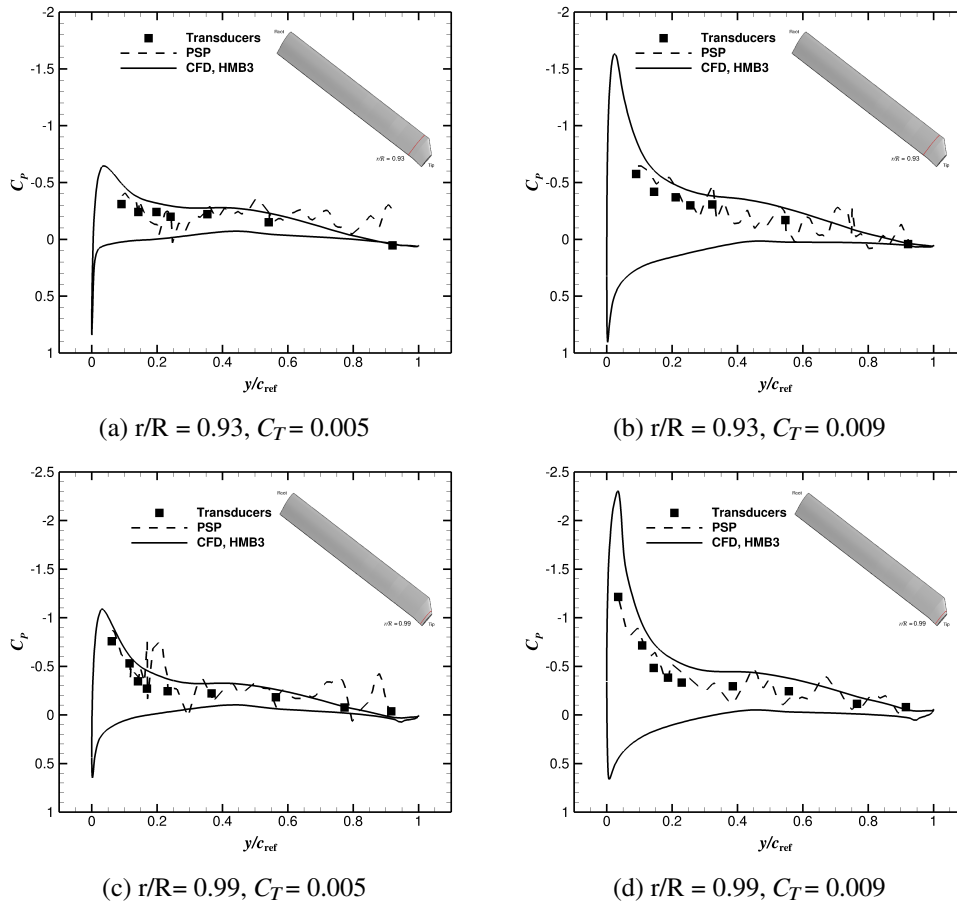


Fig. 14 C_p profile comparisons between experimental data using the PSP technique (dashed line) and pressure tap (square symbols) [41, 42] and CFD (solid line) at radial stations $r/R = 0.93$ and $r/R = 0.99$.

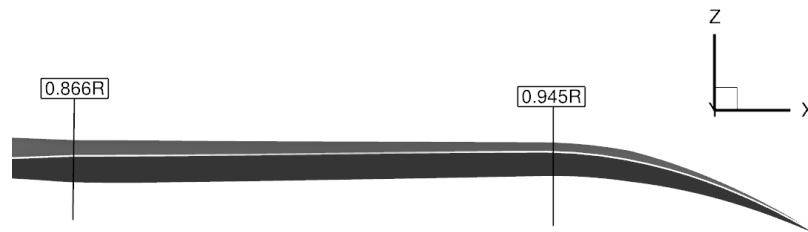


Fig. 15 Geometry of the Langley BERP blade with 15 deg parabolic anhedral, viewed in the streamwise direction.

blade. The performance improvement due to anhedral, comes from a small increase in thrust and torque reduction. Of course, no experimental data exists to validate this results, however, the benefit of blade anhedral was also seen for other rotor blades such as the S-76 rotor blade [9]. To examine the sources of the beneficial action of anhedral, the surface pressure distributions and sectional loads are compared. The surface pressure distribution for the Langley BERP and Baseline blades with and without anhedral are shown in Figure 16. The pressure coefficient is normalised by local flow velocity.

Table 11 Hover performance comparison of standard Langley Baseline and Langley BERP rotors, and blade with 15 degrees parabolic anhedral.

Blade	C_T	C_Q	FoM	FoM % improvement
LBL	0.00885	0.000880	0.6702	-
LBL with 15 deg anhedral	0.00891	0.000849	0.6997	+4.4%
LBERP	0.00882	0.000934	0.6276	-
LBERP with 15 deg anhedral	0.00888	0.000883	0.6698	+6.7%

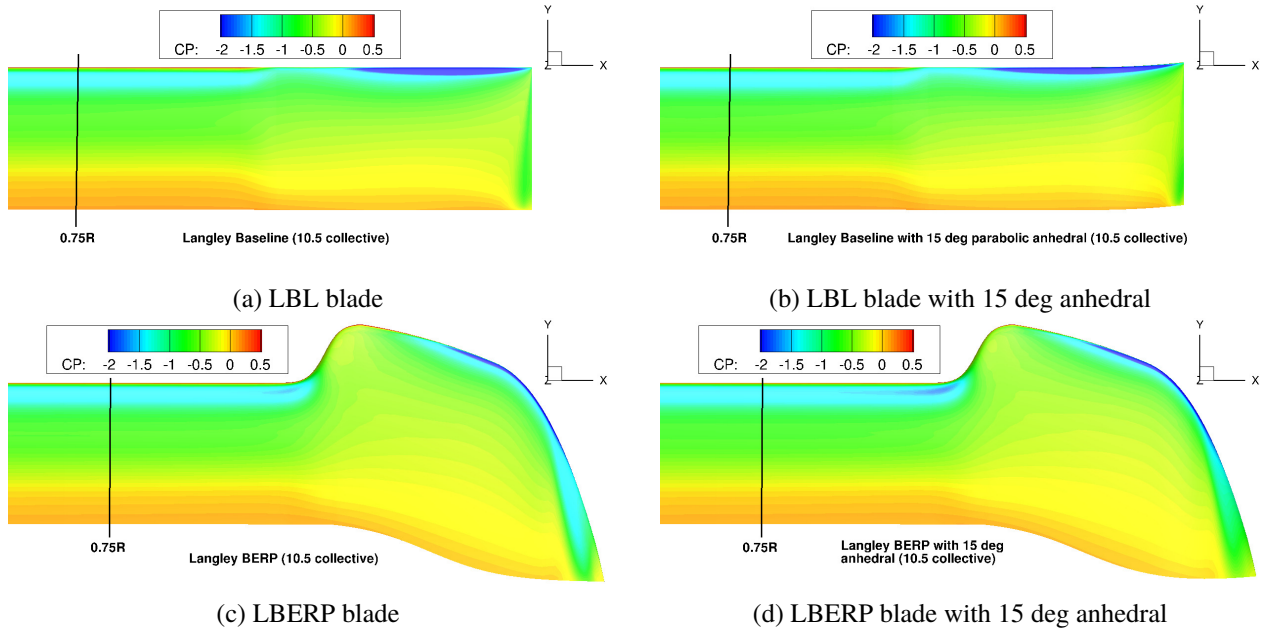


Fig. 16 Comparison of surface pressure distributions (normalised by local flow velocity) for the Langley Baseline and BERP blades in hover with and without anhedral.

The anhedral is found to redistribute the loading along the blade leading to an offloading of the blade tip and higher loading inboard. This leads to a more optimal induced lift distribution and reduced overall torque. In fact, the blade anhedral acts similarly as additional negative twist on the blade loading distribution. **Similar findings were reported in [16, 25, 66, 67].** The differences in blade loading for the blades with and without anhedral are noticeably lower for the Langley Baseline blade. The aerofoil transition region, can also be clearly seen in the surface pressure distributions, where the pressure iso-lines spread out. For the Langley BERP blade, a reduced suction at the blade tip can be observed (caused by formation of the tip vortex). The suction, however, is increased in the blade notch region. This is highlighted further through the sectional load distributions, in Figure 17.

The observations from the surface pressure distributions are confirmed by the sectional load distributions. The anhedral has a similar effect on the rotor thrust distributions, where a larger amount of thrust is generated inboard. The benefit of anhedral, mainly comes from a reduction in torque at the blade tip, which is seen for both blades. For the Langley BERP tip, the largest reduction can be seen across the paddle-like blade tip, as well as at the very end of

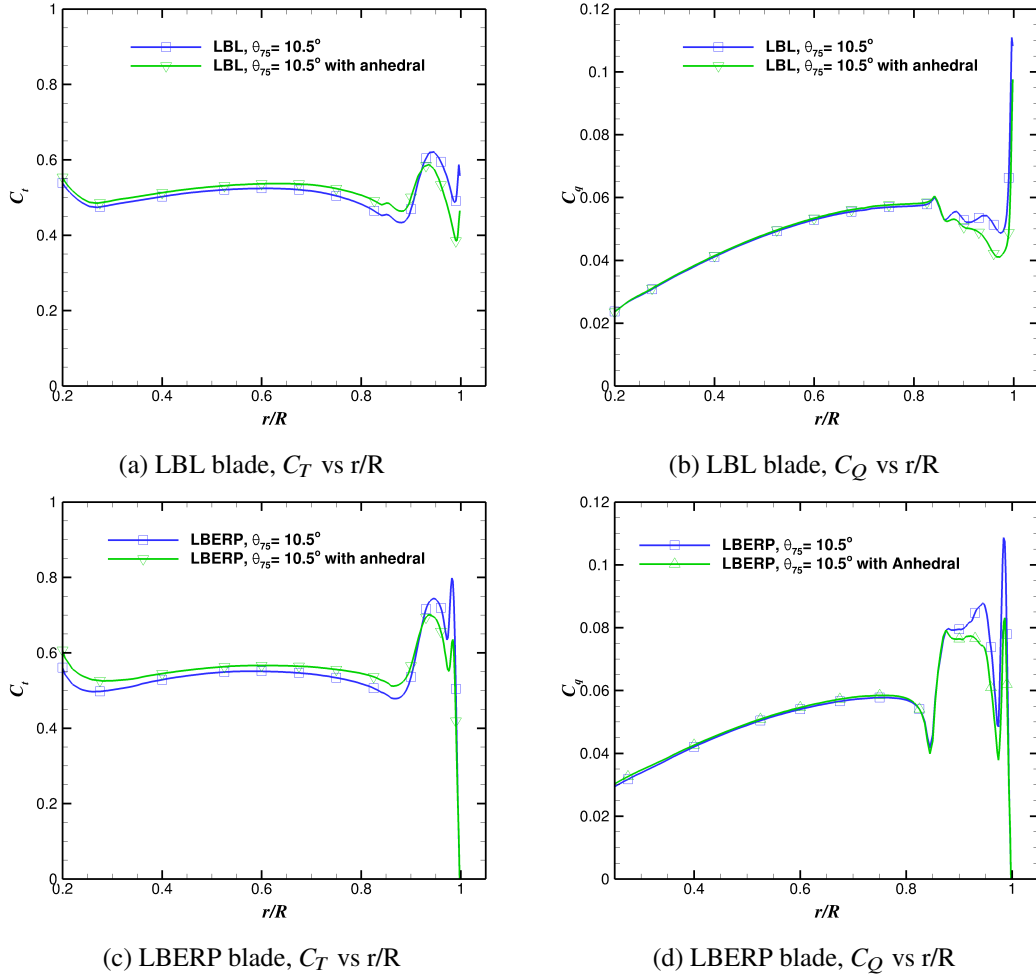


Fig. 17 Comparison of sectional load distributions (normalised by local flow velocity and reference blade chord taken as the chord of the first aerodynamic section) for the Langley Baseline and BERP blades in hover with and without anhedral.

the tip where the tip vortex forms. For the Langley Baseline blade, the torque is reduced past the aerofoil transition region. The differences in the blade loading can be explained by the fact that the preceding blade vortex induces more tangential velocities relative to the blade surface for a blade with anhedral. **The benefits of anhedral are usually stronger for highly loaded blades [3]. The LBERP generates a stronger downwash field in the blade tip region compared to a rectangular blade, and hence has a greater performance improvement when anhedral is integrated into the blade design.** The effects of anhedral show that advanced planforms require careful computational optimisation. This is due to the strong sensitivity of geometric features such as anhedral on the blade performance, as shown for the Langley Baseline and BERP blades.

Conclusions

This paper demonstrates the capability of a steady-state CFD method to accurately predict the hover performance for a number of different rotor blades within the design envelope. Four rotor geometries with different planform geometries were simulated within this paper at a variety of flight conditions. The main conclusions are:

- The steady state CFD method is able to obtain very good performance predictions regardless of planform geometry, disk loading and blade tip Mach number with limited computational resources. The rotor **FoM** can be predicted within 1 count for most cases with grid sizes of approximately 10 million cells.
- To reach a **FoM** CFD prediction within 0.1 counts, more accurate validation data is required. Experimental data currently available in literature has a large degree of scatter, and hence, the use of more advanced CFD methods is not fully justified. Furthermore, full-scale flight test data and hover performance data for advanced planforms is extremely scarce, but necessary to improve current CFD prediction capabilities
- Blade anhedral is a geometric feature of the blade that has a strong effect on the rotor performance, and was found to be more beneficial for the Langley BERP blade compared to the conventional Langley Baseline geometry. This result shows, that advanced planforms require careful computational optimisation to fully take advantage of potential benefits due to planform shape.
- Compared to the unsteady CFD method, the steady state formulation is able to achieve similar results, and due to reduced computational time is more suitable for industrial use. Contrarily, for stalled rotor blades the unsteady formulation would be more appropriate.
- To further improve the predictions, higher order schemes and adaptive mesh refinement should be used to reduce the **numerical diffusion leading to a more efficient discretisation of the computational domain and better representation of the rotor wake properties.**
- **Finally, to consider cases at high thrust coefficients where the steady state formulation is not applicable, and simulations including the fuselage, spectral methods should be considered as an alternative to much more expensive time accurate computations.**

Acknowledgements

This work is funded by DSTL (Defence Science and Technology Laboratory), Contract No. 74260. A part of the technical work has been completed under the collaboration project, TTCP AER CP13.A1, Next Generation Rotor Blade Design. Results were obtained using the EPSRC funded ARCHIE-WeSt High Performance Computer (www.archie-west.ac.uk). EPSRC grant no. EP/K000586/1. This work used the Cirrus UK National Tier-2 HPC Service at EPCC (<http://www.cirrus.ac.uk>).

References

- [1] Chaderijan, N., “Advances in Rotor Performance and Turbulent Wake Simulation using DES and Adaptive Mesh Refinement,” *Seventh International Conferences on Computational Fluid Dynamics (ICCFD7)*, Big Island, Hawaii, 2012.
- [2] Johnson, C., “Optimisation of Aspects of Rotor Blades using Computational Fluid Dynamics,” Ph.D. thesis, University of Liverpool, 2012.
- [3] Brocklehurst, A., and Barakos, G., “A review of helicopter rotor blade tip shapes,” *Progress in Aerospace Sciences*, Vol. 56, 2013, pp. 35 – 74. DOI:10.1016/j.paerosci.2012.06.003.
- [4] BG. van der Wall and C. Kessler and Y. Delrieux and P. Beaumier and M. Gervais and JF. Hirsch and K. Pengel and P. Crozier, “From Aeroacoustics Basic Research to a Modern Low-Noise Rotor Blade,” *Journal of the American Helicopter Society*, Vol. 62, No. 4, 2017, pp. 1–16. DOI:10.4050/JAHS.62.042001.
- [5] Boeing, “New Chinook Composite Blades Proven,” <http://www.boeing.com/features/2017/01/chinook-blades-01-17.page>, 2017. [Online; accessed 19-June-2019].
- [6] Landgrebe, A. J., “The Wake Geometry of a Hovering Rotor and its Influence on Rotor Performance,” *Journal of the American Helicopter Society*, Vol. 17, No. 4, 1972, pp. 3–15. DOI: 10.4050/JAHS.17.3.
- [7] Kocurek, J. D., and Tangler, J. L., “A Prescribed Wake Lifting Surface Hover Performance Analysis,” *Journal of the American Helicopter Society*, Vol. 22, No. 1, 1977, pp. 24–35. DOI: 10.4050/JAHS.22.24.
- [8] Hariharan, N., Egolf, T., and Sankar, L., “Simulation of Rotor in Hover: Current State and Challenges,” *AIAA SciTech Forum, 52th Aerospace Sciences Meeting*, National Harbor, Maryland, 2014.
- [9] Balch, D., and J.Lombardi, “Experimental Study of Main Rotor Tip Geometry and Tail Rotor Interactions in Hover, Vol I - Text and Figures,” Tech. rep., National Aeronautics and Space Administration, 1985. NASA-CR-177336-Vol-1.
- [10] Hariharan, N., Narducci, R., Reed, E., and Egolf, T., “Helicopter Aerodynamic Modeling of Rotor with Tip-Shape Variations: AIAA Standardized Hover Evaluations,” *AIAA SciTech Forum, 54th Aerospace Sciences Meeting*, San Diego, California, 2016.
- [11] Egolf, T., Hariharan, N., Narducci, R., and Reed, E., “AIAA Standardized Hover Simulation: Hover Performance Prediction Status and Outstanding Issues,” *AIAA SciTech Forum, 55th Aerospace Sciences Meeting*, Grapevine, Texas, 2017.
- [12] Overmeyer, A. D., and and, P. B. M., “Measured Boundary Layer Transition and Rotor Hover Performance at Model Scale,” *AIAA SciTech Forum 55th Aerospace Sciences Meeting*, Grapevine, Texas, 2017.
- [13] Sheng, C., “Role of Transition Modeling in Rotor Hover Predictions,” *Journal of Aircraft*, Vol. 55, No. 1, 2018, pp. 23–37. DOI: 10.2514/1.C034137.
- [14] Sheng, C., Wang, J., and Zhao, Q., “Improved Rotor Hover Predictions Using Advanced Turbulence Modeling,” *Journal of Aircraft*, Vol. 53, No. 4, 2016, pp. 1549–1560. DOI: 10.2514/1.C033512.

- [15] Sheng, C., Zhao, Q., and Hill, M., “Computational Investigation of a Full-Scale Proprotor Hover Performance and Flow Transition,” *Journal of Aircraft*, Vol. 55, No. 1, 2018, pp. 122–132. DOI: 10.2514/1.C034015.
- [16] Jain, R., “Hover Predictions on the S-76 Rotor with Tip Shape Variation Using Helios,” *Journal of Aircraft*, Vol. 55, No. 1, 2018, pp. 66–77. DOI: 10.2514/1.C034075.
- [17] Jain, R., “CFD Performance and Turbulence Transition Predictions of an Installed Model-scale Rotor in Hover,” *AIAA SciTech Forum, 55th Aerospace Sciences Meeting*, Grapevine, Texas, 2017.
- [18] Jain, R., “Effect of Facility Walls and Blade Aeroelasticity on PSP Rotor Hover Performance Predictions,” *AIAA SciTech Forum, 56th Aerospace Sciences Meeting*, Kissimmee, Florida, 2018.
- [19] Jimenez-Garcia, A., and Barakos, G. N., “CFD Analysis of Hover Performance of Rotors at Full-and Model-Scale Conditions,” *The Aeronautical Journal*, Vol. 120, No. 1, 2016, pp. 1386–1424. DOI: 10.1017/aer.2016.58.
- [20] Jain, R., “Sensitivity Study of High-Fidelity Hover Predictions on the Sikorsky S-76 Rotor,” *Journal of Aircraft*, Vol. 55, No. 1, 2018, pp. 78–88. DOI: 10.2514/1.C034076.
- [21] Abras, J., and Harihran, N., “Comparison of Computational Fluid Dynamics Hover Predictions on the S-76 Rotor,” *Journal of Aircraft*, Vol. 55, No. 1, 2018, pp. 12–22. DOI: 10.2514/1.C034121.
- [22] Lakshminarayan, V., Sitaraman, J., and Wissink, A., “Sensitivity fo Rotorcraft Hover Predictions to Mesh Resolution in Strand Grid Framework,” *AIAA Journal*, 2019. Article in Advance, DOI: 10.2514/1.J056571.
- [23] Holst, T., and Puliam, T., “Overset Solution Adaptive Grid Approach Applied to Hovering Rotorcraft Flows,” *27th AIAA Applied Aerodynamics Conference*, San Antonio, Texas, 2009.
- [24] Jacobson, K., and Smith, M., “Carefree Hybrid Methodology for Rotor Hover Performance Analysis,” *Journal of Aircraft*, Vol. 55, No. 1, 2018, pp. 52–65. DOI: 10.2514/1.C034112.
- [25] Min, B., and Wake, B., “Modified Hybrid Navier–Stokes/Free-Wake Method for Hovering Rotor Analysis,” *Journal of Aircraft*, Vol. 55, No. 1, 2018, pp. 38–51. DOI: 10.2514/1.C034066.
- [26] Narducci, R., “Comparison of Steady-State and Time-Dependent Solutions for the S-76 Model-Scale Rotor in Hover,” *AIAA SciTech Forum, 55th Aerospace Sciences Meeting*, Grapevine, Texas, 2017.
- [27] GR. Whitehouse, D. W., and Quackenbush, T., “Predicting the Influence of Blade Shape on Hover Performance with Comprehensive Analyses,” *Journal of Aircraft*, Vol. 55, No. 1, 2018, pp. 111–121. DOI: 10.2514/1.C034073.
- [28] Leon, E., Le Pape, A., Desideri, J., Alfano, D., and Costes, M., “Concurrent Aerodynamic Optimization of Rotor Blades Using a Nash Game Method,” *Journal of the American Helicopter Society*, Vol. 61, No. 2, 2016, pp. 1–13. DOI: 10.4050/JAHS.61.022009.
- [29] Imiela, M., “High-fidelity optimization framework for helicopter rotors,” *Journal of Aerospace Science and Technology*, Vol. 23, No. 1, 2012, pp. 2–16. DOI: 10.1016/j.ast.2011.12.011.

- [30] Le Pape, A., and Beaumier, P., “Numerical Optimization of Helicopter Rotor Aerodynamic Performance in Hover,” *Journal of Aerospace Science and Technology*, Vol. 9, No. 3, 2005, pp. 191–201. DOI: 10.1016/j.ast.2004.09.004.
- [31] Dumont, A., Le Pape, A., Peter, J., and Huberson, S., “Aerodynamic Shape Optimization of Hovering Rotors Using a Discrete Adjoint of the Reynolds-Averaged Navier-Stokes Equations,” *Journal of the American Helicopter Society*, Vol. 56, No. 3, 2011, pp. 1–11. DOI: 10.4050/JAHS.56.032002.
- [32] McCluer, M., and Johnson, J., “Full-Span Tiltrotor Aeroacoustic Mdoel (FS TRAM) - Overview and Initial Testing,” *American Helicopter Society Aerodynamics, Acoustics, and Test and Evaluation Technical Specialists’ Meeting*, San Francisco, California, 2002.
- [33] Shinoda, P., Yeo, H., and Norman, T., “Rotor Performance of a UH-60 Rotor System in the NASA Ames 80- by 120-Foot Wind Tunnel,” *American Helicopter Society 58th Annual Forum*, Montreal, Canada, 2002.
- [34] Roesch, P., “Aerodynamic Design of the Aerospatiale SA 365N Dauphin 2 Helicopter,” *Journal of the American Helicopter Society*, Vol. 27, No. 2, 1982, pp. 27–33. DOI: 10.4050/JAHS.27.27.
- [35] Polz, G., and Schimke, D., “New Aerodynamic Rotor Blade Design at MBB,” *Thirteenth European Rotorcraft Forum*, Arles, France, 1987.
- [36] Morris, P., Ottomeyer, J., Higgins, L., Bender, G., Picasso III, B., and Savage, R., “Airworthiness and Flight Characteristics Test - Part I, YAH-64 Attack Helicopter,” Tech. rep., United States Army Engineering Flight Activity, 1981. USAAEFA NO. 80-17-1.
- [37] Caradonna, F., and Tung, C., “Experimental and Analytical Studies of a Model Helicopter Rotor in Hover,” Tech. rep., National Aeronautics and Space Administration, 1982. NASA/TM-81232.
- [38] Lorber, P., “Aerodynamic Results of a Pressure-Instrumented Model Rotor Test at the DNW,” *Journal of the American Helicopter Society*, Vol. 36, No. 4, 1991, pp. 66–76. DOI: 10.4050/JAHS.36.66.
- [39] Steijl, R., Barakos, G. N., and Badcock, K., “A framework for CFD analysis of helicopter rotors in hover and forward flight,” *International Journal for Numerical Methods in Fluids*, Vol. 51, No. 8, 2006, pp. 819–847. DOI: 10.1002/d.1086.
- [40] Dehaeze, F., and Barakos, G., “Hovering rotor computations using an aeroelastic blade model,” *The Aeronautical Journal*, Vol. 116, No. 1180, 2011, pp. 621–649. DOI: 10.1017/S0001924000007107.
- [41] Wong, O., Noonan, K., Watkins, A., Jenkins, L., and Yao, C., “Non-Intrusive Measurements of a Four-Bladed Rotor in Hover - A First Look,” *American Helicopter Society Aeromechanics Specialists Conference*, San Francisco, California, 2010.
- [42] Wong, O., Watkins, A., Goodman, K., Crafton, J., Forlines, A., Goss, L., Gregory, J., and Juliano, T., “Blade Tip Pressure Measurements using Pressure Sensitive Paint,” *Journal of the American Helicopter Society*, Vol. 63, No. 1, 2018, pp. 1–11. DOI: 10.4050/JAHS.63.012001.

- [43] Yeager Jr, W., Noonan, K., Singleton, J., Wilbur, M., and Mirick, P., "Performance and Vibratory Loads Data From a Wind-Tunnel Test of a Model Helicopter Main-Rotor Blade With a Paddle-Type Tip," Tech. rep., National Aeronautics and Space Administration, 1997. NASA-TM-4754.
- [44] Betzina, M., "Rotor Performance of an Isolated Full-Scale XV-15 Tiltrotor in Helicopter Mode," *American Helicopter Society Aerodynamics, Acoustics, and Test and Evaluation Technical Specialist Meeting*, San Francisco, CA, 2002.
- [45] Jimenez-Garcia, A., and Barakos, G. N., "Accurate Predictions of Rotor Hover Performance at Low and High Disc Loadings," *Journal of Aircraft*, Vol. 55, No. 1, 2018, pp. 89–110. DOI: 10.2514/1.C034144.
- [46] Steijl, R., and Barakos, G. N., "Sliding mesh algorithm for CFD analysis of helicopter rotor-fuselage aerodynamics," *International Journal for Numerical Methods in Fluids*, Vol. 58, No. 5, 2008, pp. 527–549. DOI: 10.1002/d.1757.
- [47] Osher, S., and Chakravarthy, S., "Upwind schemes and boundary conditions with applications to Euler equations in general geometries," *Journal of Computational Physics*, Vol. 50, No. 3, 1983, pp. 447–481. DOI: 10.1016/0021-9991(83)90106-7.
- [48] van Leer, B., "Towards the ultimate conservative difference scheme. V.A second-order sequel to Godunov's Method," *Journal of Computational Physics*, Vol. 32, No. 1, 1979, pp. 101–136. DOI: 10.1016/0021-9991(79)90145-1.
- [49] van Albada, G. D., van Leer, B., and Roberts, W. W., "A Comparative Study of Computational Methods in Cosmic Gas Dynamics," *Astronomy and Astrophysics*, Vol. 108, No. 1, 1982, pp. 76–84. DOI: 10.1007/978-3-642-60543-7_6.
- [50] Axelsson, O., *Iterative Solution Methods*, Cambridge University Press: Cambridge, MA, 1994. DOI: 10.1017/CBO9780511624100.
- [51] Jarkowski, M., Woodgate, M., Barakos, G. N., and Rokicki, J., "Towards consistent hybrid overset mesh methods for rotorcraft CFD," *International Journal for Numerical Methods in Fluids*, Vol. 74, No. 8, 2014, pp. 543–576. DOI: 10.1002/fld.3861.
- [52] Menter, F. R., "Two-Equation Eddy-Viscosity Turbulence Models for Engineering Applications," *AIAA Journal*, Vol. 32, No. 8, 1994, pp. 1598–1605. DOI: 10.2514/3.12149.
- [53] Menter, F. R., Smirnov, P. E., Liu, T., and Avancha, R., "A One-Equation Local Correlation-Based Transition Model," *Flow Turbulence Combust*, Vol. 95, No. 4, 2015, pp. 583–619. DOI:10.1007/s10494-015-9622-4.
- [54] Colonia, S., Leble, V., Steijl, R., and Barakos, G., "Assessment and Calibration of the γ -Equation Transition Model for a Wide Range of Reynolds Numbers at Low Mach," *AIAA Journal*, Vol. 55, No. 4, 2017, pp. 1126–1139. DOI: 10.2514/1.J055403.
- [55] Noonan, K. W., "Aerodynamic Characteristics of Two Rotorcraft Airfoils Designed for Application to the Inboard Region of a Main Rotor Blade," NASA TP-3009, U.S. Army Aviation Systems Command, TR-90-B-005, 1990.
- [56] Noonan, K. W., "Aerodynamic Characteristics of Two Rotorcraft Airfoils Designed for Application to the Inboard Region of a Main Rotor Blade," NASA TM-4264, U.S. Army Aviation Systems Command, TR-91-B-003, 1991.

- [57] Felker, F. F., Betzina, M. D., and Signor, D. B., "Performance and Loads Data from a Hover Test of a Full-Scale XV-15 Rotor," NASA TM-86833, Sep. 1985.
- [58] Amer, K., "Technical Note: High Speed Rotor Aerodynamics," *Journal of American Helicopter Society*, Vol. 34, No. 1, 1989, pp. 63-63. DOI: 10.4050/JAHS.34.63.
- [59] Perry, F., "Technical Note: The Contribution of Planform Area to the Performance of the BERP Rotor (Reply to Kenneth B. Amer)," *Journal of American Helicopter Society*, Vol. 34, No. 1, 1989, pp. 64-65. DOI: 10.4050/JAHS.34.64.
- [60] Wilcox, D., "Formulation of the k-omega Turbulence Model Revisited," *AIAA journal*, Vol. 46, No. 11, 2008, pp. 2823-2838. DOI: 10.2514/1.36541.
- [61] Vieira, B., Kinzel, M., and Maughmer, M., "CFD Hover Predictions Including Boundary-Layer Transition," *55th Aerospace Sciences Meeting*, Grapevine, Texas, 2017.
- [62] Light, J. S., "Results from an XV-15 Rotor Test in the National Full-Scale Aerodynamics Complex," *53rd Annual Forum of the American Helicopter Society*, Virginia Beach, Virginia, 1997.
- [63] Scott, M., Sigl, D., and Strawn, R., "Computational and Experimental Evaluation of Helicopter Rotor Tips for High-Speed Flight," *Journal of Aircraft*, Vol. 28, No. 6, 1991, pp. 403-409. DOI: 10.2514/3.46041.
- [64] Perry, F., "Aerodynamics of the World Speed Record," *43rd Annual Forum of the American Helicopter Society*, St. Louis, Missouri, 1987.
- [65] Makofski, R., "Charts for estimating the hovering endurance of a helicopter," NACA TN 3810, Langley Aeronautical Laboratory, Oct. 1956.
- [66] Smith, M., Jacobson, K., Grubb, A., Wachspress, D., and Whitehouse, G., "Evaluation of Rotor Hover Performance With Differing Blade Tip Shapes Using A Carefree Hybrid Methodology," *AIAA SciTech Forum, 53rd Aerospace Sciences Meeting*, Kissimmee, Florida, 2015.
- [67] Narducci, R., "Hover Performance Assessment of Several Tip Shapes using OVERFLOW," *AIAA SciTech Forum, 53rd Aerospace Sciences Meeting*, Kissimmee, Florida, 2015.